Identification of non-parametric probabilistic models from measured transfer functions

M. Arnst, Didier Clouteau, Marc Bonnet

Inversion of probabilistic structural models using measured transfer functions ⋆

M. Arnst* [a], D. Clouteau [a], M. Bonnet [b],

[a] *MSSMat, UMR8579, Ecole Centrale Paris, Grande Voie des Vignes, F-92295 Châtenay-Malabry Cedex, France. Fax:+33 1 41 13 14 42. Tel:+33 1 41 13 13 59.*

[b] *LMS, UMR7649, Ecole Polytechnique, F-91128 Palaiseau Cedex, France. Fax:+33 1 69 33 30 26.*

Abstract

This paper addresses the inversion of probabilistic models for the dynamical behaviour of structures using experimental data sets of measured frequency-domain transfer functions. The inversion is formulated as the minimization, with respect to the unknown parameters to be identified, of an objective function that measures a distance between the data and the model. Two such distances are proposed, based on either the loglikelihood function, or the relative entropy. As a comprehensive example, a probabilistic model for the dynamical behaviour of a slender beam is inverted using simulated data. The methodology is then applied to a civil and environmental engineering case history involving the identification of a probabilistic model for ground-borne vibrations from real experimental data.

Key words: probabilistic modelling, inverse problem, identification, relative entropy, likelihood, non-parametric probabilistic model

1 Introduction

Predictive models for the dynamical behaviour of complex structures are inevitably confronted to data uncertainties and modelling errors. Uncertain data include material properties, geometric parameters and boundary conditions. Modelling errors are introduced by the assumptions and approximations made in the modelling process. The data uncertainties and modelling errors may sometimes result in significant uncertainties in the model predictions. Probabilistic models then are desirable, since

⋆ *Comp. Meth. Appl. Mech, Engng.* **197**:589–608 (2008)
Email address: maarten.arnst@ecp.fr (M. Arnst*).

Preprint submitted to

they provide a way to quantify the impact of the data uncertainties and modelling errors on the predictions.

At low frequencies, deterministic models most often allow accurate predictions of the dynamic response of a structure. The low-frequency response is governed by only a few global eigenmodes so that the sensitivity of the response to data uncertainties and modelling errors is low. Upon updating the model by appropriate methods [1–3], the predictions usually compare very well with experiments. However, the sensitivity of the response is known to increase with the frequency [4]. At medium and high frequencies, the data uncertainties and modelling errors must therefore be taken into account and their propagation to the predictions must be modelled.

Several probabilistic approaches have been proposed in the literature, see e.g. the reviews [5–8]. Parametric probabilistic models accommodate uncertainty by modelling the local physical features of a structural model (i.e. its geometrical parameters, fields of material properties and boundary conditions) by random variables and/or fields, see e.g. [5, 9, 10]. Non-parametric probabilistic models incorporate uncertainty by modelling global features of a structural model by random variables. An example is the non-parametric approach proposed by Soize [11, 12], where reduced matrix models of structures are defined in terms of random matrices. Models of this last kind can incorporate a large class of uncertainties, including data uncertainties and modelling errors.

A central problem in the practical construction of a probabilistic structural model is the choice of the probability distribution of the random variables, fields or matrices. This probability distribution should be chosen on the basis of only the available information, which typically consists of experimental data (such as measurements of the dynamical response of the real structure under study) and of the essential mathematical or physical properties that the probabilistic model should possess (such as positiveness, symmetry or invertibility, depending on the quantity that is being modelled).

A general approach consists in representing the probability distribution of the random variables, fields or matrices in a versatile manner as a function of a large number of parameters. For example, it can be represented by a truncated polynomial chaos expansion, whereby the coefficients of this expansion make up the large set of parameters of the probability distribution, see e.g. [9, 13–15]. These parameters should then be identified from the available information. An inherent difficulty associated to this approach is that the identification of such a large set of parameters may be difficult in practice (ill-posedness, computational cost).

Soize [11, 12, 16] has presented an alternative approach whereby the essential mathematical properties are explicitly used to build the probability distribution of the random variables, fields or matrices. That probability distribution is chosen, which maximizes entropy [17–19] under the constraint that the mathematical properties

should be fulfilled. This principle of construction allows obtaining probability distributions parameterized by the mean value of the random variables, fields or matrices, and by a minimal set of essential parameters (such as spatial correlation lengths and dispersion levels). A key advantage is that their experimental identification can generally be formulated as a well-posed inverse problem that is numerically solvable with a reasonable computational effort.

This article investigates the inversion of non-parametric probabilistic structural models with minimal parameterization using experimental data sets of measured frequency-domain Transfer Functions (TFs). Experimental data of this kind are often used in more classical inverse problems involving the identification of deterministic structural models, see e.g. [20]. Among their advantages over time-domain TFs are the possibility to select data in a specific frequency range of interest and the relatively easy characterization of the distortion of the data due to experimental noise [3]. Compared to modal data, they have the advantage that they can also be used in medium-frequency range problems.

Within the theory of mathematical statistics, methods for solving stochastic inverse problems are studied and developed, see e.g. the standard texts [21–26]. Three stochastic inverse methods, often called the classical methods of estimation, are well-established and frequently used, namely the method of moments, the method of maximum likelihood and the Bayes estimation method. Several authors have applied these classical methods to the inversion of probabilistic models of mechanical structures, see e.g. [2, 16, 27–37]. Moreover, the method of moments has been applied to the identification of stochastic models for fields of material properties of heterogeneous geophysical domains, see e.g. [38–40].

In this article, it will be shown that the classical methods of estimation from the theory of mathematical statistics, in particular the method of maximum likelihood, are not well-adapted to the experimental identification of probabilistic structural models from measured TFs. Computational difficulties, and conceptual problems due to the potential incompatibility of the experimental data and the probabilistic model, will be shown to hinder the application of the classical methods. To overcome these difficulties, an alternative formulation of the inverse problem will then be proposed as the minimization, with respect to the unknown parameters to be identified, of an objective function that measures a distance between the experimental data and the probabilistic model. The main objective of this article is to investigate how this distance can be defined and computed suitably. Two distances, respectively based on the loglikelihood function and on the entropy entropy [22, 41, 42], will be formulated and then demonstrated on examples featuring simulated and real experimental data.

The following notations are frequently used in this article. Any vector $\boldsymbol{x} = (x_1, \ldots, x_n)$ is identified with the $(n \times 1)$ column matrix of its components. Let $\mathbb{K}$ be $\mathbb{R}$ or $\mathbb{C}$. The space $\mathrm{M}_{m\times n}(\mathbb{K})$ is the space of $(m \times n)$ matrices $\boldsymbol{X}$ whose entries $X_{k\ell}$ are in $\mathbb{K}$. If $m = n$, $\mathrm{M}_{n\times n}(\mathbb{K})$ is denoted simply by $\mathrm{M}_n(\mathbb{K})$, and $\mathrm{M}_n^+(\mathbb{K})$ is the space of Hermitian positive definite matrices. The determinant of matrix $\boldsymbol{X} \in \mathrm{M}_n(\mathbb{K})$ is denoted by $\det(\boldsymbol{X})$ and its trace by $\mathrm{tr}(\boldsymbol{X}) = \sum_{k=1}^n X_{kk}$. The transpose of $\boldsymbol{X} \in \mathrm{M}_{m\times n}(\mathbb{K})$ is denoted by $\boldsymbol{X}^{\mathrm{T}}$ and its adjoint by $\boldsymbol{X}^\star = \overline{\boldsymbol{X}}^{\mathrm{T}}$, where $\overline{\boldsymbol{X}}$ denote the complex conjugate of $\boldsymbol{X}$. The Frobenius norm of $\boldsymbol{X} \in \mathrm{M}_{m\times n}(\mathbb{K})$ is defined by $||\boldsymbol{X}||_{\mathrm{F}} = \sqrt{\mathrm{tr}\,(\boldsymbol{X}\boldsymbol{X}^\star)}$.

2 Problem setting

It is assumed that the dynamical behaviour of a single real structure is under study. Any structural model is usually an imperfect representation of the dynamical behaviour of this real structure for two reasons. First, there may be parameter uncertainty in that there may be a lack of knowledge of the geometrical parameters, material properties and boundary conditions. Nominal values are then usually assigned, which may imperfectly characterize the real structure. Second, modelling errors may have been introduced by simplifying approximations made in the modelling process, either stemming from a poor understanding of the dynamical behaviour of the real structure, or being deliberately introduced to reduce the model complexity. Examples of potential modelling errors are linearization, the use of simple constitutive laws, or the use of simplified models for joints. Upon considering a single real structure, there is, in principle, no data variability. Were a collection of similar, but not perfectly identical, real structures considered instead, the data uncertainties would also result from variability in these features, due to dispersion in the manufacturing process.

This article concerns the experimental identification of a non-parametric probabilistic structural model such that the probability distribution of its random predictions as adequately as possible represents the uncertainty in these predictions resulting from parameter uncertainty and modelling errors. This probability distribution should be viewed as a representation of the imperfect knowledge of the dynamical behaviour of the real structure. Since only a single structure is considered, it cannot be viewed as a representation of a variability in the dynamical behaviour.

3 The data set and the probabilistic structural model

This section introduces a generic experimental data set and a probabilistic structural model, which will be used in the next section to set up inverse methods.

3.1 The data set

The real structure is assumed to be instrumented by means of n_{M} transducers located on its boundary. The dynamical behaviour is studied by applying a broadband time-limited pressure field on a small portion of the boundary and by measuring the induced mechanical motion in the n_{M} experimental Degrees Of Freedom (DOFs). It is assumed that this experiment is repeated n_{R} times. The repetition of the experiment ($n_{\mathrm{R}} > 1$) is useful in regard of the experimental noise which may disturb the measurement of the applied force and the induced mechanical response. The noise may concern the mechanical motion of the structure due to parasite excitations, electrical noise in the transducers and the wires and discretization errors. Under some assumptions, the repetition of the experiment allows recovering, from the noisy measurement data, those data which would be obtained if the vibration test were not disturbed by noise, see e.g. [3]. Moreover, it allows estimating the coherence function to quantify the level of distortion of the experimental data due to noise, see e.g. [3].

3.1.1 Experimental data

The raw measurement data consist of a time-dependent applied force and of time-dependent responses measured in n_{M} experimental DOFs for n_{R} repetitions of the experiment. Accordingly, let $\tilde{f}_r^{\mathrm{obs}}(t)$ and $\tilde{u}_{rm}^{\mathrm{obs}}(t)$ denote the measured applied force and response at the m-th sensor, respectively, for the r-th repetition. These data are sampled in the time domain and, subsequently, transformed into the frequency domain by means of the Discrete Fourier Transform to obtain:

$$\{\tilde{f}_r^{\mathrm{obs}}(\omega_\ell) \mid 1 \leq \ell \leq n_{\mathrm{F}} \ , \ 1 \leq r \leq n_{\mathrm{R}}\} \quad , \tag{1}$$

$$\{\tilde{u}_{rm}^{\mathrm{obs}}(\omega_\ell) \mid 1 \leq \ell \leq n_{\mathrm{F}} \ , \ 1 \leq r \leq n_{\mathrm{R}} \ , \ 1 \leq m \leq n_{\mathrm{M}}\} \quad , \tag{2}$$

where $\{\omega_\ell \mid 1 \leq \ell \leq n_{\mathrm{F}}\}$ is the set of n_{F} discrete frequencies. The value taken by the observed TF for the m-th sensor and the r-th repetition at the frequency ω_ℓ is defined as the frequency-domain ratio of the measured response and applied force:

$$\tilde{h}_{rm}^{\mathrm{obs}}(\omega_\ell) = \frac{\tilde{u}_{rm}^{\mathrm{obs}}(\omega_\ell)}{\tilde{f}_r^{\mathrm{obs}}(\omega_\ell)}. \tag{3}$$

These values are gathered in the data set

$$\widetilde{\boldsymbol{D}}^{\text{obs}} = \{\tilde{\boldsymbol{h}}_1^{\text{obs}}(\omega_\ell), \ldots, \tilde{\boldsymbol{h}}_{n_{\text{R}}}^{\text{obs}}(\omega_\ell) \mid 1 \leq \ell \leq n_{\text{F}}\} \quad , \tag{4}$$

where the values taken by the n_{M} observed TFs for the r-th repetition at the frequency ω_ℓ are gathered in the vector $\tilde{\boldsymbol{h}}_r^{\text{obs}}(\omega_\ell) \in \mathbb{C}^{n_{\text{M}}}$.

3.1.2 The noise-free idealization

When the vibration test is not disturbed by noise, the experiment is carried out only once ($n_{\text{R}} = 1$). A data set

$$\boldsymbol{D}^{\text{obs}} = \{\boldsymbol{h}^{\text{obs}}(\omega_\ell) \mid 1 \leq \ell \leq n_{\text{F}}\} \tag{5}$$

is then obtained collecting the values taken by the noise-free TFs at the n_{F} discrete frequencies. The m-th component $h_m^{\text{obs}}(\omega_\ell)$ is the frequency-domain ratio of the undisturbed response in the m-th transducer and the applied force at the discrete frequency ω_ℓ.

3.2 The probabilistic structural model

The non-parametric probabilistic model is built on the basis of a deterministic reduced matrix model for the dynamical analysis of the structure. Only fixed structures are considered here, so that the reduction basis does not contain rigid-body modes. More general cases are presented e.g. in [37].

3.2.1 The deterministic reduced matrix model

A deterministic reduced matrix model is built to predict the TFs of the structure in the frequency band of analysis $B = [\omega_{\min}, \omega_{\max}],\ 0 < \omega_{\min} < \omega_{\max}$. It is assumed that the structure under consideration is modelled by a linear time-invariant damped Finite Element (FE) model, written in the frequency domain as:

$$[\boldsymbol{K}_{\text{h}} + i\omega\boldsymbol{D}_{\text{h}} - \omega^2\boldsymbol{M}_{\text{h}}]\boldsymbol{u}_{\text{h}}(\omega) = \boldsymbol{f}_{\text{h}}(\omega) \ , \quad \omega \in B. \tag{6}$$

The matrices $\boldsymbol{K}_{\text{h}}, \boldsymbol{D}_{\text{h}}, \boldsymbol{M}_{\text{h}} \in \text{M}_{n_{\text{h}}}^+(\mathbb{R})$, where n_{h} is the number of FE DOFs, are the stiffness, damping and mass matrices, and are independent of ω over B. For a fixed ω, $\boldsymbol{u}_{\text{h}}(\omega)$ and $\boldsymbol{f}_{\text{h}}(\omega)$ collect the FE DOFs and nodal forces.

If the frequency band B corresponds to the low-frequency range, reduced matrix models can be built by projecting (6) onto subsets of dynamical eigenmodes, see e.g. [43]. If B belongs to the medium-frequency range, specific reduction bases are needed, following e.g. the approaches of Soize [44] or Sarkar and Ghanem [45].

Let an appropriate reduction basis of dimension n_{T} (with $n_{\mathrm{T}} \ll n_{\mathrm{h}}$ usually) be defined through the transformation matrix $\boldsymbol{T} \in \mathrm{M}_{n_{\mathrm{h}} \times n_{\mathrm{T}}}(\mathbb{R})$. The deterministic reduced matrix model related to $\boldsymbol{T}$ is then defined by

$$[\boldsymbol{K} + i\omega\boldsymbol{D} - \omega^2\boldsymbol{M}]\boldsymbol{q}(\omega) = \boldsymbol{T}^{\mathrm{T}}\boldsymbol{f}_{\mathrm{h}}(\omega)\ , \quad \omega \in B \quad , \tag{7}$$

$$\boldsymbol{u}(\omega) = \boldsymbol{T}\boldsymbol{q}(\omega) \quad , \tag{8}$$

where $\boldsymbol{K} = \boldsymbol{T}^{\mathrm{T}}\boldsymbol{K}_{\mathrm{h}}\boldsymbol{T}$, $\boldsymbol{D} = \boldsymbol{T}^{\mathrm{T}}\boldsymbol{D}_{\mathrm{h}}\boldsymbol{T}$, $\boldsymbol{M} = \boldsymbol{T}^{\mathrm{T}}\boldsymbol{M}_{\mathrm{h}}\boldsymbol{T} \in \mathrm{M}^{+}_{n_{\mathrm{T}}}(\mathbb{R})$ are the reduced stiffness, damping and mass matrices, respectively. For a fixed ω, $\boldsymbol{q}(\omega)$ is the vector of the generalized coordinates, and $\boldsymbol{u}(\omega)$ approximates the solution $\boldsymbol{u}_{\mathrm{h}}(\omega)$ of (6). The positive definiteness of the reduced matrices ensures the existence, uniqueness and continuity with respect to the nodal forces $\boldsymbol{f}_{\mathrm{h}}(\omega)$ of the solution of (7)-(8).

Let the r-th measured applied force at the discrete frequency ω_ℓ have the FE discretization $\boldsymbol{f}_{\mathrm{h}r}(\omega_\ell) = \boldsymbol{b}_{\mathrm{h}}\tilde{f}^{\mathrm{obs}}_r(\omega_\ell)$, where $\boldsymbol{b}_{\mathrm{h}}$ is the input shape vector. It is assumed here that each experimental DOF m corresponds to a single FE DOF j. Accordingly, let $\boldsymbol{C}$ denote the $n_{\mathrm{h}} \times n_{\mathrm{M}}$ sensor output matrix, whose entries are $C_{jm} = \delta(j-m)$, where δ is the Dirac distribution. The n_{M} deterministic TF values at the discrete frequency ω_ℓ are then gathered in the complex vector $\boldsymbol{h}(\omega_\ell; \boldsymbol{K}, \boldsymbol{D}, \boldsymbol{M})$ defined by:

$$\boldsymbol{h}(\omega_\ell; \boldsymbol{K}, \boldsymbol{D}, \boldsymbol{M}) = \boldsymbol{C}^{\mathrm{T}}\boldsymbol{T}[\boldsymbol{K} + i\omega_\ell\boldsymbol{D} - \omega_\ell^2\boldsymbol{M}]^{-1}\boldsymbol{T}^{\mathrm{T}}\boldsymbol{b}. \tag{9}$$

Finally, let the mapping γ symbolize the correspondence between the reduced matrices and the deterministic TF values at all discrete frequencies:

$$\gamma : \left(\mathrm{M}^{+}_{n_{\mathrm{T}}}(\mathbb{R})\right)^3 \to \mathbb{C}^{n_{\mathrm{M}} \times n_{\mathrm{F}}} : (\boldsymbol{K}, \boldsymbol{D}, \boldsymbol{M}) \mapsto \gamma(\boldsymbol{K}, \boldsymbol{D}, \boldsymbol{M}) = \{\boldsymbol{h}(\omega_\ell; \boldsymbol{K}, \boldsymbol{D}, \boldsymbol{M}) \mid 1 \leq \ell \leq n_{\mathrm{F}}\}. \tag{10}$$

3.2.2 Construction of the non-parametric probabilistic model

The non-parametric probabilistic model is built by replacing the reduced matrices of model (7)-(8) by random matrices. Since the TFs depend non-linearly on the reduced matrices, the complete probability distribution of these random matrices must be defined to be able to compute statistics of the random TFs (the definition of e.g. only their second order moments would not be sufficient). This paragraph summarizes the methodology of Soize [11, 12] for the construction of this probability law.

Let the random matrices replacing $\boldsymbol{K}$, $\boldsymbol{D}$ and $\boldsymbol{M}$ be denoted by $\mathbb{K}(\boldsymbol{p})$, $\mathbb{D}(\boldsymbol{p})$ and $\mathbb{M}(\boldsymbol{p})$. They are defined on a probability measure space $(\mathcal{A}, \mathcal{T}, P)$ (where $\mathcal{A}$ is a sample space of outcomes, $\mathcal{T}$ a σ-algebra of events, and $P : \mathcal{T} \to [0,1]$ a probability measure), have values in $\mathrm{M}^{+}_{n_{\mathrm{T}}}(\mathbb{R})$ and are parameterized by the parameter set $\boldsymbol{p} = \{\boldsymbol{p}_0, \boldsymbol{p}_\delta\}$, which gathers mean model parameters $\boldsymbol{p}_0$ and dispersion parameters $\boldsymbol{p}_\delta$, to be defined next.

Soize's construction assumes the knowledge of the mean values of the random matri-

ces. Let the mean reduced matrices be denoted by $\underline{\boldsymbol{K}}(\boldsymbol{p}_0), \underline{\boldsymbol{D}}(\boldsymbol{p}_0), \underline{\boldsymbol{M}}(\boldsymbol{p}_0) \in \mathrm{M}^+_{n_\mathrm{T}}(\mathbb{R})$:

$$E\left\{\mathbb{K}(\boldsymbol{p})\right\} = \underline{\boldsymbol{K}}(\boldsymbol{p}_0),\ E\left\{\mathbb{D}(\boldsymbol{p})\right\} = \underline{\boldsymbol{D}}(\boldsymbol{p}_0),\ E\left\{\mathbb{M}(\boldsymbol{p})\right\} = \underline{\boldsymbol{M}}(\boldsymbol{p}_0) \quad , \tag{11}$$

where $E\left\{\cdot\right\}$ denotes the mathematical expectation. The mean model parameters $\boldsymbol{p}_0$ may consist of local properties of the model (e.g. material properties, geometrical characteristics or boundary conditions), or of global characteristics (e.g. eigenfrequencies), see Section 7 for an example.

Each random matrix $\mathbb{A}(\boldsymbol{p})$ (where $\mathbb{A}$ denotes any of $\mathbb{K}$, $\mathbb{D}$ or $\mathbb{M}$) is written in the following form:

$$\mathbb{A}(\boldsymbol{p}) = \underline{L}_\mathrm{A}(\boldsymbol{p}_0)^\mathrm{T}\mathbb{N}_\mathrm{A}(\delta_\mathrm{A})\underline{L}_\mathrm{A}(\boldsymbol{p}_0) \quad \text{with} \quad \underline{\boldsymbol{A}}(\boldsymbol{p}_0) = \underline{L}_\mathrm{A}(\boldsymbol{p}_0)^\mathrm{T}\underline{L}_\mathrm{A}(\boldsymbol{p}_0). \tag{12}$$

Each matrix $\underline{L}_\mathrm{A}(\boldsymbol{p}_0)$ is the Cholesky factor of the corresponding matrix $\underline{\boldsymbol{A}}(\boldsymbol{p}_0)$. Each normalized random matrix $\mathbb{N}_\mathrm{A}(\delta_\mathrm{A})$ is independent, defined on $(\mathcal{A}, \mathcal{T}, P)$, valued in $\mathrm{M}^+_{n_\mathrm{T}}(\mathbb{R})$ and parameterized by a dispersion parameter $\delta_\mathrm{A} \in \mathbb{R}^+_0$ such that

$$\delta_\mathrm{A}^2 = \frac{E\left\{||\mathbb{N}_\mathrm{A}(\delta_\mathrm{A}) - \boldsymbol{I}||_\mathrm{F}^2\right\}}{E\left\{||\boldsymbol{I}||_\mathrm{F}^2\right\}} = \frac{E\left\{||\mathbb{N}_\mathrm{A}(\delta_\mathrm{A}) - \boldsymbol{I}||_\mathrm{F}^2\right\}}{n_A}. \tag{13}$$

The set of dispersion parameters $\boldsymbol{p}_\delta$ is therefore defined as $\boldsymbol{p}_\delta = \{\delta_\mathrm{K}, \delta_\mathrm{D}, \delta_\mathrm{M}\}$. An analytical expression for the probability law of $\mathbb{N}_\mathrm{A}$ has been obtained [11, 12] by entropy maximization [17–19, 42] subject to the following constraints:

- $\mathbb{N}_\mathrm{A}(\delta_\mathrm{A}) \in \mathrm{M}^+_{n_\mathrm{T}}(\mathbb{R})$.
- $\mathbb{N}_\mathrm{A}(\delta_\mathrm{A})$ is of the second order and its mean value is the identity matrix $\boldsymbol{I}$:

$$E\left\{\mathbb{N}_\mathrm{A}(\delta_\mathrm{A})\right\} = \boldsymbol{I}. \tag{14}$$

- $\mathbb{N}_\mathrm{A}(\delta_\mathrm{A})$ fulfills the condition:

$$\left|E\left\{\log\left(\det\left(\mathbb{N}_\mathrm{A}(\delta_\mathrm{A})\right)\right)\right\}\right| < +\infty \quad , \tag{15}$$

in order to ensure that the following important invertibility property holds:

$$E\left\{\left|\left|\mathbb{N}_\mathrm{A}(\delta_\mathrm{A})^{-1}\right|\right|_\mathrm{F}^2\right\} < +\infty. \tag{16}$$

Requirement (16) is found to be fulfilled [11, 12] if δ_A satisfies:

$$0 < \delta_\mathrm{A} < \sqrt{(n_\mathrm{T}+1)/(n_\mathrm{T}+5)} < 1. \tag{17}$$

Upon replacing the reduced matrices $\boldsymbol{K}$, $\boldsymbol{D}$ and $\boldsymbol{M}$ in model (7)-(8) by the random reduced matrices $\mathbb{K}(\boldsymbol{p})$, $\mathbb{D}(\boldsymbol{p})$ and $\mathbb{M}(\boldsymbol{p})$, a non-parametric probabilistic model,

parameterized by $\boldsymbol{p}$, is obtained of the form:

$$\Big[\mathbb{K}(\boldsymbol{p}) + i\omega\mathbb{D}(\boldsymbol{p}) - \omega^2\mathbb{M}(\boldsymbol{p})\Big]\mathbb{Q}(\omega;\boldsymbol{p}) = \boldsymbol{T}^{\mathrm{T}}\boldsymbol{f}_{\mathrm{h}}(\omega)\ , \quad \omega \in B \quad , \tag{18}$$

$$\mathbb{U}(\omega;\boldsymbol{p}) = \boldsymbol{T}\mathbb{Q}(\omega;\boldsymbol{p}). \tag{19}$$

The stochastic processes $\{\mathbb{Q}(\omega;\boldsymbol{p}) \mid \omega \in B\}$ and $\{\mathbb{U}(\omega;\boldsymbol{p}) \mid \omega \in B\}$, defined on $(\mathcal{A}, \mathcal{T}, P)$, indexed on B and with respective values in $\mathbb{C}^{n_{\mathrm{T}}}$ and $\mathbb{C}^{n_{\mathrm{h}}}$, are the random generalized coordinates and the random FE DOFs, respectively. The positive definiteness of the random reduced matrices implies that the random problem (18)-(19) is well-posed. If

$$\forall\omega \in B : ||\boldsymbol{f}_{\mathrm{h}}(\omega)||^2 < +\infty \quad , \tag{20}$$

and the dispersion parameters $\boldsymbol{p}_\delta$ satisfy inequality (17), the invertibility properties (16) of the random reduced matrices allow to show [12] that the random structure response $\{\mathbb{U}(\omega;\boldsymbol{p}) \mid \omega \in B\}$ is a second-order stochastic process:

$$\forall\omega \in B : E\left\{||\mathbb{U}(\omega;\boldsymbol{p})||^2\right\} < +\infty. \tag{21}$$

The theoretical properties of, and the computational tools for, second-order random variables (e.g. convergence properties and the central limit theorem) can then be used.

The probabilistic model (18)-(19) determines a set of n_{M} random TFs corresponding to the deterministic TFs defined in (9). These random TFs are the image of the random matrices through the deterministic mapping γ defined in (10). They are collected in the stochastic process $\{\mathbb{H}(\omega_\ell, \boldsymbol{p}) \mid 1 \leq \ell \leq n_{\mathrm{F}}\}$, defined on $(\mathcal{A}, \mathcal{T}, P)$, indexed on $\{1 \leq \ell \leq n_{\mathrm{F}}\}$, valued in $\mathbb{C}^{n_{\mathrm{M}}}$ and of the second order:

$$\{\mathbb{H}(\omega_\ell;\boldsymbol{p}) \mid 1 \leq \ell \leq n_{\mathrm{F}}\} = \gamma\Big(\mathbb{K}(\boldsymbol{p}), \mathbb{D}(\boldsymbol{p}), \mathbb{M}(\boldsymbol{p})\Big). \tag{22}$$

The stochastic process $\{\mathbb{H}(\omega_\ell;\boldsymbol{p}) \mid 1 \leq \ell \leq n_{\mathrm{F}}\}$ is assumed to admit a system of cylindrical PDFs. The n-th order cylindrical PDF, defined as the joint PDF of n random variables $\{\mathbb{H}(\omega_{\ell_1};\boldsymbol{p}), \ldots, \mathbb{H}(\omega_{\ell_n};\boldsymbol{p})\}$, is denoted by $\theta^{(n)}\left(\cdot\middle|\omega_{\ell_1}, \ldots, \omega_{\ell_n};\boldsymbol{p}\right) : \mathbb{C}^{n_{\mathrm{M}}\times n} \to \mathbb{R}^+$.

4 The stochastic inverse problem

In the previous section, a generic experimental data set of observed TFs was defined, and a non-parametric probabilistic structural model was built. The inversion of this probabilistic model using experimental data of this kind is the subject of this section.

4.1 The method of maximum likelihood and the relative entropy

The definitions of the method of maximum likelihood and the relative entropy are now briefly recalled. Let $\boldsymbol{x} = \{x_r \mid 1 \leq r \leq n_{\mathrm{R}}\}$ be a set of n_{R} independent and identically-distributed (iid) observations of a generic random variable $\mathbb{X}$ with values in $\mathbb{C}$. Let the set $\{f(x|\boldsymbol{p}) \mid \boldsymbol{p} \in P\}$ be a collection of candidate PDFs, defined on $\mathbb{C}$ and parameterized by $\boldsymbol{p} \in P \subset \mathbb{R}^n$, intended to model the probability distribution of $\mathbb{X}$. The likelihood of the parameters $\boldsymbol{p}$ given the observations $\boldsymbol{x}$ is defined by:

$$L(\boldsymbol{p}) = \prod_{r=1}^{n_{\mathrm{R}}} f(x_r|\boldsymbol{p}). \tag{23}$$

The method of maximum likelihood consists in choosing a parameter point [46]

$$\hat{\boldsymbol{p}} = \arg\max_{\boldsymbol{p}\in P} L(\boldsymbol{p}) \quad , \tag{24}$$

i.e. such that the observed samples are most likely.

Let f_1 and f_2 be two PDFs with supports $T \subset \mathbb{C}^m$ and $S \subset \mathbb{C}^m$, respectively, where $T \subset S$. The relative entropy from f_1 to f_2 is then defined by [22, 41]:

$$\mathcal{I}(f_1||f_2) = \int_T f_1(\boldsymbol{x}) \log \frac{f_1(\boldsymbol{x})}{f_2(\boldsymbol{x})} d\boldsymbol{x} \quad , \tag{25}$$

and can be interpreted as a distance-like measure of the separation between the PDFs f_1 and f_2. However, since it does not in general satisfy the symmetry property and the triangle inequality, it is not a true metric distance. It should be noted that there exist many other functionals which allow measuring the separation between PDFs, see e.g. [47].

4.2 Difficulties in the application of the maximum likelihood principle

When the vibration test has been carried out under noise-free conditions, the maximum likelihood estimate reads:

$$\hat{\boldsymbol{p}} = \arg\max_{\boldsymbol{p}} \theta^{(n_{\mathrm{F}})}(\boldsymbol{D}^{\mathrm{obs}}|\omega_1, \ldots, \omega_{n_{\mathrm{F}}}; \boldsymbol{p}). \tag{26}$$

Considerable difficulties may arise in this application of the method of maximum likelihood, as explained next.

4.2.1 Potentially prohibitive computational cost

The first difficulty comes from a numerical issue. The following two-step procedure could be proposed for the numerical approximation of the likelihood of a fixed $\boldsymbol{p}$:

- **Step 1:** Generate a set of iid samples of the stochastic process $\{\mathbb{H}(\omega_\ell;\boldsymbol{p}) \mid 1 \leq \ell \leq n_\mathrm{F}\}$.
- **Step 2:** Compute the likelihood of $\boldsymbol{p}$ by estimating the value taken by the PDF $\theta^{(n_\mathrm{F})}(\cdot|\cdot;\boldsymbol{p})$ at the data set $\boldsymbol{D}^\mathrm{obs}$ from these samples using a numerical density estimation method (Sec. 5).

However, it is well known, see e.g. [48], that the computational effort required to numerically approximate a PDF grows rapidly with the dimension of the sample space, equal here to $2 \times n_\mathrm{M} \times n_\mathrm{F}$. The numerical solution of (26) is therefore impractical when n_M or n_F is large, which is often the case in vibration tests.

4.2.2 Potential incompatibility of the model and the data

The second difficulty stems from the fact that the probabilistic structural model may be incompatible with the experimental data: observed TFs $\boldsymbol{D}^\mathrm{obs}$ that lie outside the support of the PDF $\theta^{(n_\mathrm{F})}(\cdot|\cdot;\boldsymbol{p})$ for any choice of $\boldsymbol{p}$ may occur.

Equation (22) means that each realisation of the predicted random TFs is the image of a realisation of the triplet of random reduced matrices, and is hence determined entirely by a finite number of coefficients, namely the entries of the matrices. The TFs of the real structure, being defined over the continuous frequency interval B, are not generally representable in terms of a fixed finite set of finite-dimensional matrices. This implies that there may in practice not exist any triplet $(\boldsymbol{K},\boldsymbol{D},\boldsymbol{M})$ such that:

$$\boldsymbol{D}^\mathrm{obs} = \gamma(\boldsymbol{K},\boldsymbol{D},\boldsymbol{M}) \quad , \tag{27}$$

i.e. such that the deterministic reduced matrix model perfectly reproduces the observed TFs. In such a situation, the observed TFs $\boldsymbol{D}^\mathrm{obs}$ lie outside the support of the PDF $\theta^{(n_\mathrm{F})}(\cdot|\cdot;\boldsymbol{p})$ irrespective of the parameter value $\boldsymbol{p}$, which prohibits the application of the maximum likelihood principle.

Such an incompatibility of the TFs of the real structure and the random TFs essentially occurs when the former and the realisations of the latter do not depend on the frequency in the same way. For a simple illustration, consider the case of a 2-DOF oscillator for which a probabilistic model is taken as a 1-DOF oscillator with random stiffness, damping and mass. All realisations of the random TF then belong to 1-DOF oscillator responses so that the frequency-dependent TF of the 2-DOF oscillator is not a realisation of the frequency-dependent random TF.

4.2.3 Potential difficulties due to experimental noise

Additional difficulties caused by distortions of the observed TFs due to experimental noise were not considered, but are to be expected. These will be addressed in Section 4.3.2.

The aforementioned difficulties motivate the development of alternative inverse methods. We propose to formulate the inversion as the minimization, with respect to the sought parameters, of an objective function that measures a distance between the observed TFs and the predicted random TFs.

4.3.1 Undisturbed vibration test

When the vibration test has been carried out under noise-free conditions, we propose to define a distance $\mathcal{L}$ as the average over the frequencies of the sign-reversed loglikelihood function:

$$\mathcal{L}(\boldsymbol{p}) = -\frac{1}{n_{\mathrm{F}}} \sum_{\ell=1}^{n_{\mathrm{F}}} \log \theta^{(1)} \left(\boldsymbol{h}^{\mathrm{obs}}(\omega_\ell) \middle| \omega_\ell; \boldsymbol{p} \right). \tag{28}$$

The unknown parameters can then be estimated from the data on the basis of $\mathcal{L}$ by

$$\hat{\boldsymbol{p}} = \arg\min_{\boldsymbol{p}} \mathcal{L}(\boldsymbol{p}). \tag{29}$$

The inverse method (29) can be written in the following equivalent form by interchanging the sum and the logarithm in (28):

$$\hat{\boldsymbol{p}} = \arg\max_{\boldsymbol{p}} \prod_{\ell=1}^{n_{\mathrm{F}}} \theta^{(1)} \left(\boldsymbol{h}^{\mathrm{obs}}(\omega_\ell) \middle| \omega_\ell; \boldsymbol{p} \right) \quad , \tag{30}$$

highlighting that it amounts to the application of the maximum likelihood principle upon replacing the predicted joint PDF for the possible values of the observed TFs by the product of the predicted first-order cylindrical PDFs.

4.3.2 Disturbed vibration test

When the vibration measurements are disturbed by experimental noise, we propose to account for the distortions in the data using a probabilistic model for the noise.

Probabilistic model for the experimental noise For a fixed frequency ω_ℓ, the observed TFs obtained for the set of n_{R} repetitions of the vibration measurement are written in the following form:

$$\begin{pmatrix} \tilde{\boldsymbol{h}}_1^{\mathrm{obs}}(\omega_\ell) \\ \vdots \\ \tilde{\boldsymbol{h}}_{n_{\mathrm{R}}}^{\mathrm{obs}}(\omega_\ell) \end{pmatrix} = \boldsymbol{h}^{\mathrm{obs}}(\omega_\ell) + \begin{pmatrix} \boldsymbol{e}_1(\omega_\ell) \\ \vdots \\ \boldsymbol{e}_{n_{\mathrm{R}}}(\omega_\ell) \end{pmatrix} \quad , \tag{31}$$

i.e. each noisy observed TF value is viewed as the sum of the noise-free TF value and a contribution of experimental noise. The n_{R} contributions $\{\boldsymbol{e}_r(\omega_\ell) \mid 1 \leq r \leq n_{\mathrm{R}}\}$ are modelled as iid realisations of a circular [3] multivariate complex Gaussian random variable $\mathbb{E}(\omega_\ell)$. Its mean value is taken vanishing, and its covariance matrix is estimated from the experimental data as:

$$\widehat{\boldsymbol{C}}^{\mathrm{obs}}(\omega_\ell) = \frac{1}{n_{\mathrm{R}}} \sum_{r=1}^{n_{\mathrm{R}}} \Big(\tilde{\boldsymbol{u}}_r^{\mathrm{obs}}(\omega_\ell) - \hat{\boldsymbol{h}}^{\mathrm{obs}}(\omega_\ell) \tilde{f}_r^{\mathrm{obs}}(\omega_\ell)\Big)\Big(\tilde{\boldsymbol{u}}_r^{\mathrm{obs}}(\omega_\ell) - \hat{\boldsymbol{h}}^{\mathrm{obs}}(\omega_\ell) \tilde{f}_r^{\mathrm{obs}}(\omega_\ell)\Big)^\star, \quad (32)$$

where $\hat{\boldsymbol{h}}^{\mathrm{obs}}(\omega_\ell)$ is the so-called $H1$-estimate of the noise-free TF value, defined by [3]:

$$\hat{\boldsymbol{h}}^{\mathrm{obs}}(\omega_\ell) = \frac{\frac{1}{n_{\mathrm{R}}} \sum_{r=1}^{n_{\mathrm{R}}} \tilde{\boldsymbol{u}}_r^{\mathrm{obs}}(\omega_\ell) \tilde{f}_r^{\mathrm{obs}}(\omega_\ell)^\star}{\frac{1}{n_{\mathrm{R}}} \sum_{r=1}^{n_{\mathrm{R}}} \left|\tilde{f}_r^{\mathrm{obs}}(\omega_\ell)\right|^2}. \quad (33)$$

The PDF of the random variable $\mathbb{E}(\omega_\ell)$ is denoted by $N(\cdot|\boldsymbol{0}, \widehat{\boldsymbol{C}}^{\mathrm{obs}}(\omega_\ell)) : \mathbb{C}^{n_{\mathrm{M}}} \to \mathbb{R}^+$, where, for $\boldsymbol{x}, \boldsymbol{\mu} \in \mathbb{C}^n$ and $\boldsymbol{C} \in \mathrm{M}_n^+(\mathbb{C})$ [3]:

$$N(\boldsymbol{x}|\boldsymbol{\mu}, \boldsymbol{C}) = \frac{1}{\pi^n \det(\boldsymbol{C})} \exp\Big(-(\boldsymbol{x}-\boldsymbol{\mu})^\star \boldsymbol{C}^{-1} (\boldsymbol{x}-\boldsymbol{\mu})\Big). \quad (34)$$

Distance on the basis of the loglikelihood function For each frequency ω_ℓ, a PDF $\varphi^{(1,n_{\mathrm{R}})}(\cdot|\omega_\ell; \boldsymbol{p}) : \mathbb{C}^{n_{\mathrm{M}} \times n_{\mathrm{R}}} \to \mathbb{R}^+$ for the set of n_{R} noisy observed TF values at that frequency is built on the basis of the probabilistic model for the dynamical behaviour of the structure and the probabilistic model for the experimental noise as:

$$\varphi^{(1,n_{\mathrm{R}})}\Big(\tilde{\boldsymbol{h}}_1, \ldots, \tilde{\boldsymbol{h}}_{n_{\mathrm{R}}}\Big|\omega_\ell; \boldsymbol{p}\Big) = \int_{\mathbb{C}^{n_{\mathrm{M}}}} \theta^{(1)}\Big(\boldsymbol{h}\Big|\omega_\ell; \boldsymbol{p}\Big) \prod_{r=1}^{n_{\mathrm{R}}} N\Big(\tilde{\boldsymbol{h}}_r|\boldsymbol{h}, \widehat{\boldsymbol{C}}^{\mathrm{obs}}(\omega_\ell)\Big) d\boldsymbol{h}. \quad (35)$$

A distance $\mathcal{L}$ is defined as the average over the frequencies of the sign-reversed loglikelihood function:

$$\mathcal{L}(\boldsymbol{p}) = -\frac{1}{n_{\mathrm{F}}} \sum_{\ell=1}^{n_{\mathrm{F}}} \log \varphi^{(1,n_{\mathrm{R}})}\left(\tilde{\boldsymbol{h}}_1^{\mathrm{obs}}(\omega_\ell), \ldots, \tilde{\boldsymbol{h}}_{n_{\mathrm{R}}}^{\mathrm{obs}}(\omega_\ell)\Big|\omega_\ell; \boldsymbol{p}\right). \quad (36)$$

The unknown parameters can then be estimated from the data on the basis of $\mathcal{L}$ by

$$\hat{\boldsymbol{p}} = \arg\min_{\boldsymbol{p}} \mathcal{L}(\boldsymbol{p}). \quad (37)$$

Distance on the basis of the relative entropy For each frequency ω_ℓ, a numerical density estimation method (Sec. 5) is used to obtain, from the experimental data, an estimate $\hat{\psi}^{(1)}(\cdot|\omega_\ell) : \mathbb{C}^{n_{\mathrm{M}}} \to \mathbb{R}^+$ of the PDF of the noisy observed TF values

at that frequency. An alternative PDF $\hat{\psi}^{(1,n_\mathrm{R})}(\cdot|\omega_\ell) : \mathbb{C}^{n_\mathrm{M}\times n_\mathrm{R}} \to \mathbb{R}^+$ for the set of n_R noisy observed TF values is then obtained as:

$$\hat{\psi}^{(1,n_\mathrm{R})}\left(\tilde{\boldsymbol{h}}_1,\ldots,\tilde{\boldsymbol{h}}_{n_\mathrm{R}}|\omega_\ell\right) = \prod_{r=1}^{n_\mathrm{R}} \hat{\psi}^{(1)}\left(\tilde{\boldsymbol{h}}_r|\omega_\ell\right). \tag{38}$$

An alternative distance $\mathcal{J}$ is defined as the average over the frequencies of the relative entropy between PDFs $\hat{\psi}^{(1,n_\mathrm{R})}(\cdot|\omega_\ell)$ and $\varphi^{(1,n_\mathrm{R})}(\cdot|\omega_\ell;\boldsymbol{p})$:

$$\mathcal{J}(\boldsymbol{p}) = \frac{1}{n_\mathrm{F}}\sum_{\ell=1}^{n_\mathrm{F}} \mathcal{I}\left(\hat{\psi}^{(1,n_\mathrm{R})}(\cdot|\omega_\ell)\middle\|\varphi^{(1,n_\mathrm{R})}(\cdot|\omega_\ell;\boldsymbol{p})\right). \tag{39}$$

The unknown parameters can then be estimated from the data on the basis of $\mathcal{J}$ by

$$\hat{\boldsymbol{p}} = \arg\min_{\boldsymbol{p}} \mathcal{J}(\boldsymbol{p}). \tag{40}$$

4.4 Expressions of the distances for Gaussian models

Let the PDFs $\theta^{(1)}(\cdot|\omega_\ell;\boldsymbol{p})$ and $\hat{\psi}^{(1)}(\cdot|\omega_\ell)$ be Gaussian:

$$\theta^{(1)}(\boldsymbol{h}|\omega_\ell;\boldsymbol{p}) = N\left(\boldsymbol{h}\middle|\boldsymbol{\mu}_0(\omega_\ell;\boldsymbol{p}),\boldsymbol{C}_0(\omega_\ell;\boldsymbol{p})\right) \quad , \tag{41}$$

$$\hat{\psi}^{(1)}\left(\tilde{\boldsymbol{h}}\middle|\omega_\ell\right) = N\left(\tilde{\boldsymbol{h}}\middle|\boldsymbol{\mu}_1(\omega_\ell),\boldsymbol{C}_1(\omega_\ell)\right) \quad , \tag{42}$$

with:

$$\boldsymbol{\mu}_1(\omega_\ell) = \frac{1}{n_\mathrm{R}}\sum_{r=1}^{n_\mathrm{R}} \tilde{\boldsymbol{h}}_r^{\mathrm{obs}}(\omega_\ell) \quad , \; \boldsymbol{C}_1(\omega_\ell) = \widehat{\boldsymbol{C}}^{\mathrm{obs}}(\omega_\ell). \tag{43}$$

For a vibration test carried out under noise-free conditions, the expression of the distance $\mathcal{L}$ corresponding to the choice (41) reads:

$$\mathcal{L}(\boldsymbol{p}) = \mathcal{L}_0 + \mathcal{L}_1(\boldsymbol{p}) + \mathcal{L}_2(\boldsymbol{p}) \quad , \tag{44}$$

$$\mathcal{L}_1(\boldsymbol{p}) = \frac{1}{n_\mathrm{F}}\sum_{\ell=1}^{n_\mathrm{F}} \left(\boldsymbol{\mu}_0(\omega_\ell;\boldsymbol{p}) - \boldsymbol{h}^{\mathrm{obs}}(\omega_\ell)\right)^\star \boldsymbol{C}_0(\omega_\ell;\boldsymbol{p})^{-1}\left(\boldsymbol{\mu}_0(\omega_\ell;\boldsymbol{p}) - \boldsymbol{h}^{\mathrm{obs}}(\omega_\ell)\right) \; ,$$

$$\mathcal{L}_2(\boldsymbol{p}) = \frac{1}{n_\mathrm{F}}\sum_{\ell=1}^{n_\mathrm{F}} \log\det \boldsymbol{C}_0(\omega_\ell;\boldsymbol{p}) \quad ,$$

where $\mathcal{L}_0$ is a constant. The term $\mathcal{L}_1$ is the weighted least-squares distance between the mean of the predicted random TFs and the noise-free observed TFs. The weighting factor is the inverse of the covariance matrix of the predicted random TF values. Hence, it attributes a smaller weight to the predictions that are more sensitive to the uncertainty introduced in the model. The mean and the covariance matrix of the predicted random TF values are primarily influenced respectively by the mean-model parameters $\boldsymbol{p}_0$ and by the dispersion parameters $\boldsymbol{p}_\delta$. The term $\mathcal{L}_1$ is expected to decrease as the dispersion parameters increase, whereas the term $\mathcal{L}_2$ is expected

to increase. Upon minimizing $\mathcal{L}$, the identification of the mean-model parameters hence essentially consists of a partial minimization of the least-squares distance $\mathcal{L}_1$, while the identified dispersion parameters achieve a balance between the reduction of $\mathcal{L}_1$ and the increment of $\mathcal{L}_2$.

For a vibration test carried out under noisy conditions, the expression of the distance $\mathcal{L}$ corresponding to the choice (41) is obtained as:

$$\mathcal{L}(\boldsymbol{p}) = \mathcal{L}_0 + \mathcal{L}_1(\boldsymbol{p}) + \mathcal{L}_2(\boldsymbol{p}) \quad , \tag{45}$$

$$\mathcal{L}_1(\boldsymbol{p}) = \frac{1}{n_{\mathrm{F}}} \sum_{\ell=1}^{n_{\mathrm{F}}} \big(\boldsymbol{\mu}_0(\omega_\ell;\boldsymbol{p}) - \boldsymbol{\mu}_1(\omega_\ell)\big)^\star \big(\boldsymbol{C}_0(\omega_\ell;\boldsymbol{p}) + \boldsymbol{C}_1(\omega_\ell)/n_{\mathrm{R}}\big)^{-1} \big(\boldsymbol{\mu}_0(\omega_\ell;\boldsymbol{p}) - \boldsymbol{\mu}_1(\omega_\ell)\big),$$

$$\mathcal{L}_2(\boldsymbol{p}) = \frac{1}{n_{\mathrm{F}}} \sum_{\ell=1}^{n_{\mathrm{F}}} \log\det\left(\boldsymbol{C}_0(\omega_\ell;\boldsymbol{p}) + \boldsymbol{C}_1(\omega_\ell)/n_{\mathrm{R}}\right) \quad ,$$

where $\mathcal{L}_0$ is a constant. The term $\mathcal{L}_1$ is the weighted least-squares distance between the mean of the predicted random TFs and the mean of the noisy observed TFs. The weighting factor features, this time, the covariance matrices of the predicted random TF values and of the noisy observed TF values. It therefore attributes a smaller weight to the predictions that are more sensitive to the uncertainty introduced in the model, and to the experimental data that are more disturbed by noise.

The expression of the distance $\mathcal{J}$ corresponding to the choices (41)-(42) reads:

$$\mathcal{J}(\boldsymbol{p}) = \mathcal{J}_0 + \mathcal{L}_1(\boldsymbol{p}) + \mathcal{L}_2(\boldsymbol{p}) + \mathcal{J}_3(\boldsymbol{p}) \quad , \tag{46}$$

$$\mathcal{J}_3(\boldsymbol{p}) = \frac{1}{n_{\mathrm{F}}} \sum_{\ell=1}^{n_{\mathrm{F}}} \left(\mathrm{tr}\left(\left(\boldsymbol{C}_0(\omega_\ell;\boldsymbol{p}) + \boldsymbol{C}_1(\omega_\ell)/n_{\mathrm{R}}\right)^{-1} \boldsymbol{C}_1(\omega_\ell)/n_{\mathrm{R}} \right) - \log\det\left(\boldsymbol{C}_1(\omega_\ell)/n_{\mathrm{R}}\right) \right),$$

where $\mathcal{J}_0$ is a constant and $\mathcal{L}_1$ and $\mathcal{L}_2$ are still defined by (45). The main difference between (45) and (46) is the presence of the term $\mathcal{J}_3$. This term is expected to have a significant influence only when the magnitude of the fluctuations of the noisy observed TFs is comparable with, or larger than, the magnitude of the fluctuations of the predicted random TFs. It then favours larger dispersion parameters.

4.5 Adequacy of the proposed inverse methods

The proposed inverse methods allow overcoming the abovementioned difficulties in the application of the method of maximum likelihood, as explained next.

4.5.1 Computational cost

Compared to the application (26) of the method of maximum likelihood, the computational cost of the proposed inverse method (29) is lower, since the former method necessitates the numerical approximation of PDFs of dimension $2 \times n_{\mathrm{M}} \times n_{\mathrm{F}}$, whereas the latter only requires the approximation of PDFs of dimension $2 \times n_{\mathrm{M}}$.

4.5.2 Incompatibility of the model and the data

It was discussed in Section 4.2.2 that the method of maximum likelihood can only be applied when the observed TFs belong to the support of the n_{F}-th order cylindrical PDF $\theta^{(n_{\mathrm{F}})}(\cdot|\cdot;\boldsymbol{p})$. This condition was found to be fulfilled if there exists a triplet of reduced matrices for which the deterministic reduced matrix model perfectly reproduces the observed TF values *concurrently at all discrete frequencies*, i.e., with reference to equation (9):

$$\exists \boldsymbol{K}, \boldsymbol{D}, \boldsymbol{M} \in \mathrm{M}^{+}_{n_{\mathrm{T}}}(\mathbb{R}) \ : \ \forall \omega_\ell \ : \ \boldsymbol{h}^{\mathrm{obs}}(\omega_\ell) = \boldsymbol{h}(\omega_\ell; \boldsymbol{K}, \boldsymbol{D}, \boldsymbol{M}). \tag{47}$$

By contrast, the distance $\mathcal{L}$, defined in (28), is already well-defined if, for each discrete frequency ω_ℓ, the observed TF value $\boldsymbol{h}^{\mathrm{obs}}(\omega_\ell)$ belongs to the support of the first-order cylindrical PDF $\theta^{(1)}(\cdot|\omega_\ell;\boldsymbol{p})$ at that frequency. This condition is fulfilled if, *at each discrete frequency* ω_ℓ *separately*, there exists a triplet of reduced matrices for which the deterministic reduced matrix model reproduces the observed TF value at that frequency, i.e.:

$$\forall \omega_\ell \ : \ \exists \boldsymbol{K}, \boldsymbol{D}, \boldsymbol{M} \in \mathrm{M}^{+}_{n_{\mathrm{T}}}(\mathbb{R}) \ : \ \boldsymbol{h}^{\mathrm{obs}}(\omega_\ell) = \boldsymbol{h}(\omega_\ell; \boldsymbol{K}, \boldsymbol{D}, \boldsymbol{M}). \tag{48}$$

The expression (48) represents a weaker condition imposed jointly on the probabilistic model and the experimental data than (47). In other words, the inverse method (29) on the basis of the distance $\mathcal{L}$ can be well-defined, even when the application of the method of maximum likelihood is prohibited by an incompatibility between the probabilistic structural model and the experimental data.

4.5.3 Prediction of frequency-dependent confidence regions

The proposed inverse methods (29), (37) and (40) are adequate for the experimental identification of probabilistic structural models intended to predict frequency-dependent confidence retions, as will be discussed in Section 6.

4.6 Bibliographical comments

The concept of solving stochastic inverse problems using only low-order cylindrical distributions is not new. Within the general framework of the theory of mathematical statistics, considerable research effort has already been devoted to developing estimation methods of this kind, see e.g. [49–53]. Restrictions to low-order cylindrical distributions are in the literature most often defended on the grounds of computational tractability.

5 Numerical resolution

Following [11, 12], computations are performed by Monte Carlo simulation. Basic algorithms are now proposed for that purpose. Algorithm 1 details the computation of a set of iid realizations of the random TFs predicted by the non-parametric probabilistic model. Then, algorithms 2, 3 and 4 detail the computation of the proposed distances.

Algorithm 1: computation with the non-parametric probabilistic model

---

- **Step 1: initialization:** choose a number n_{S} of Monte Carlo samples and $\boldsymbol{p}$.
- **Step 2: simulation of the samples of the random reduced matrices:** simulate [11, 12] a set $\left\{\left(\boldsymbol{K}_s, \boldsymbol{D}_s, \boldsymbol{M}_s\right) \mid 1 \leq s \leq n_{\mathrm{S}}\right\}$ of n_{S} iid samples of the triplet $(\mathbb{K}(\boldsymbol{p}), \mathbb{D}(\boldsymbol{p}), \mathbb{M}(\boldsymbol{p}))$.
- **Step 3: calculation of the samples of the random TFs:** for each $s \in \{1 \leq s \leq n_{\mathrm{S}}\}$ and $\ell \in \{1 \leq \ell \leq n_{\mathrm{F}}\}$, calculate, with reference to equations (9), (10) and (22):

$$\boldsymbol{h}_s(\omega_\ell) = \boldsymbol{C}^{\mathrm{T}}\boldsymbol{T}[\boldsymbol{K}_s + i\omega_\ell \boldsymbol{D}_s - \omega_\ell^2 \boldsymbol{M}_s]^{-1}\boldsymbol{T}^{\mathrm{T}}\boldsymbol{b}. \tag{49}$$

Algorithm 2: computation of the distance $\mathcal{L}$, noise-free data

---

- **Step 1: initialization:** obtain the experimental data set $\boldsymbol{D}^{\mathrm{obs}}$ and choose $\boldsymbol{p}$.
- **Step 2: computation with the non-parametric probabilistic model:** apply algorithm 1 to obtain the set of iid samples $\boldsymbol{h}_s(\omega_\ell)$ of the random TFs.
- **Step 3: numerical approximation of the distance:** for each $\ell \in \{1 \leq \ell \leq n_{\mathrm{F}}\}$, apply a density estimation method to obtain, from the samples $\{\boldsymbol{h}_s(\omega_\ell) \mid 1 \leq s \leq n_{\mathrm{S}}\}$, an estimate $\hat{\theta}^{(1)}\left(\boldsymbol{h}^{\mathrm{obs}}(\omega_\ell)\middle|\omega_\ell; \boldsymbol{p}\right)$ of the value taken by the PDF $\theta^{(1)}(\cdot|\omega_\ell; \boldsymbol{p})$ at the observed TF value $\boldsymbol{h}^{\mathrm{obs}}(\omega_\ell)$. Evaluate $\mathcal{L}$ by

$$\mathcal{L}\left(\boldsymbol{p}\right) \simeq -\frac{1}{n_{\mathrm{F}}} \sum_{\ell=1}^{n_{\mathrm{F}}} \log \hat{\theta}^{(1)}\left(\boldsymbol{h}^{\mathrm{obs}}(\omega_\ell)\middle|\omega_\ell; \boldsymbol{p}\right). \tag{50}$$

Algorithm 3: computation of the distance $\mathcal{L}$, noisy data

---

- **Step 1: initialization:** obtain the experimental data set $\tilde{\boldsymbol{D}}^{\mathrm{obs}}$ and choose $\boldsymbol{p}$.
- **Step 2: identification of the probabilistic model for the noise:** for each $\ell \in \{1 \leq \ell \leq n_{\mathrm{F}}\}$, estimate the covariance matrix $\widehat{\boldsymbol{C}}^{\mathrm{obs}}(\omega_\ell)$ using (32)-(33) .
- **Step 3: computation with the probabilistic structural model:** apply algorithm 1 to obtain the set of iid samples $\boldsymbol{h}_s(\omega_\ell)$ of the random TFs.

- **Step 4: numerical approximation of the distance:** evaluate $\mathcal{L}$ by:

$$\mathcal{L}(\boldsymbol{p}) \simeq -\frac{1}{n_{\mathrm{F}}} \sum_{\ell=1}^{n_{\mathrm{F}}} \log \frac{1}{n_{\mathrm{S}}} \sum_{s=1}^{n_{\mathrm{S}}} \prod_{r=1}^{n_{\mathrm{R}}} N\Big(\tilde{\boldsymbol{h}}_r^{\mathrm{obs}}(\omega_\ell) \Big| \boldsymbol{h}_s(\omega_\ell), \widehat{\boldsymbol{C}}^{\mathrm{obs}}(\omega_\ell)\Big). \tag{51}$$

Algorithm 4: computation of the distance $\mathcal{J}$

- **Step 1: initialization:** choose a number n_{J} of Monte Carlo samples, obtain the experimental data set $\tilde{\boldsymbol{D}}^{\mathrm{obs}}$ and choose $\boldsymbol{p}$.
- **Step 2: identification of the probabilistic model for the noise:** apply step 2 of algorithm 3 to obtain the set of covariance matrices $\widehat{\boldsymbol{C}}^{\mathrm{obs}}(\omega_\ell)$.
- **Step 3: computation with the probabilistic structural model:** apply algorithm 1 to obtain the set of iid samples $\boldsymbol{h}_s(\omega_\ell)$ of the random TFs.
- **Step 4: numerical approximation of the distance:** for each $\ell \in \{1 \leq \ell \leq n_{\mathrm{F}}\}$, apply a density estimation method to obtain, from the data $\{\tilde{\boldsymbol{h}}_r^{\mathrm{obs}}(\omega_\ell) \mid 1 \leq r \leq n_{\mathrm{R}}\}$, an estimate $\hat{\psi}^{(1)}(\cdot|\omega_\ell)$ of the PDF of the noisy TF values at the frequency ω_ℓ. Then, simulate a set $\{\tilde{\boldsymbol{h}}_{rj}(\omega_\ell) \mid 1 \leq r \leq n_{\mathrm{R}}\ ,\ 1 \leq j \leq n_{\mathrm{J}}\}$ of $n_{\mathrm{R}} \times n_{\mathrm{J}}$ iid samples of a random variable admitting this PDF $\hat{\psi}^{(1)}(\cdot|\omega_\ell)$. Evaluate $\mathcal{J}$ by:

$$\mathcal{J}(\boldsymbol{p}) \simeq \frac{1}{n_{\mathrm{F}}} \sum_{\ell=1}^{n_{\mathrm{F}}} \frac{1}{n_{\mathrm{J}}} \sum_{j=1}^{n_{\mathrm{J}}} \log \frac{\prod_{r=1}^{n_{\mathrm{R}}} \hat{\psi}^{(1)}\big(\tilde{\boldsymbol{h}}_{rj}(\omega_\ell)|\omega_\ell\big)}{\frac{1}{n_{\mathrm{S}}} \sum_{s=1}^{n_{\mathrm{S}}} \prod_{r=1}^{n_{\mathrm{R}}} N\big(\tilde{\boldsymbol{h}}_{rj}(\omega_\ell)|\omega_\ell; \boldsymbol{h}_s(\omega_\ell)\big)}. \tag{52}$$

Algorithms 2 and 4 require the estimation of PDFs from sets of samples. Density estimation methods are surveyed in [48]. The kernel density estimation method, see e.g. [48, 54, 55], is used in this work. Methods for the simulation of random variables, required in algorithm 4, are surveyed in [56]. To numerically solve the optimization problems (29), (37) and (40), we suggest applying an exhaustive grid-search when the dimension of the parameter space is three or less. Otherwise, considering that the distances to be minimized may have multiple local minima and that it may be difficult to accurately calculate gradients with respect to the parameters, we suggest applying global-search gradient-free optimization methods. The simulated annealing method [56–58] and the genetic optimization method [59, 60] are natural choices. The former is used in this work.

6 Practical methodology

We now describe a practical methodology for the identification of probabilistic structural models, which implements the above introduced theoretical and numerical tools.

6.1 Practical aim of the inverse methodology

As a working frame, the practical aim of the inverse methodology is defined as identifying the probabilistic structural model such that, upon using the identified model to predict a TF of the real structure, a frequency-dependent confidence region associated with a high probability level for the predicted random TF can be viewed as a region within which the TF of the real structure lies.

6.2 Frequency-dependent confidence regions

A methodology for constructing frequency-dependent confidence regions for predicted random TFs, which is also used in [12], is now presented. Let $\{\mathbb{X}(\omega) \mid \omega \in B\}$ be a generic random TF, being a stochastic process indexed by the frequency band B and with values in $\mathbb{C}$. A confidence region associated with a given probability level P_c for the value taken by this random TF at a fixed frequency ω on a logarithmic scale is then defined as a pair of bounds $(dB^-(\omega), dB^+(\omega))$ such that:

$$P\left(dB^-(\omega) < d\mathbb{B}(\omega) < dB^+(\omega)\right) \geq P_c \quad , \tag{53}$$

where:

$$d\mathbb{B}(\omega) = \frac{20}{\log 10} \log\left(\frac{|\mathbb{X}(\omega)|}{X^{\text{ref}}}\right) \quad , \tag{54}$$

in which X^{ref} is a reference value, equal to 1m/N, 1mHz/N or 1mHz^2/N depending on whether $\mathbb{X}(\omega)$ is a compliance (i.e. a displacement over a force), a mobility (i.e. a velocity over a force) or an inertance (i.e. an acceleration over a force), respectively. These confidence bounds are obtained using the Chebychev equation as follows:

$$dB^+(\omega) = \frac{20}{\log 10} \log\left(\frac{|E\{\mathbb{X}(\omega)\}| + a(\omega)}{X^{\text{ref}}}\right) \quad , \tag{55}$$

$$dB^0(\omega) = \frac{20}{\log 10} \log\left(\frac{|E\{\mathbb{X}(\omega)\}|}{X^{\text{ref}}}\right) \quad , \tag{56}$$

$$dB^-(\omega) = 2dB^0(\omega) - dB^+(\omega) \quad , \tag{57}$$

where:

$$a(\omega)^2 = \frac{E\{|\mathbb{X}(\omega) - E\{\mathbb{X}(\omega)\}|^2\}}{(1 - P_c)}. \tag{58}$$

6.3 Proposed practical inverse methodology

We propose to apply the inverse method (29) for an undisturbed vibration test, and either (37) or (40) for a disturbed vibration test.

For an undisturbed vibration test, the proposed inverse method (29) is expected to lead to the identification of a probabilistic model for which the observed TF values lie within the corresponding predicted confidence bounds. Indeed, considering that the observed TF values $\boldsymbol{h}^{\mathrm{obs}}(\omega_\ell)$ at a fixed frequency ω_ℓ can be expected to lie within the confidence bounds when the first-order cylindrical PDF $\theta^{(1)}(\cdot|\omega_\ell;\boldsymbol{p})$ takes a large value at $\boldsymbol{h}^{\mathrm{obs}}(\omega_\ell)$, this property follows from the fact that the sign-reversed logarithm in expression (28) strongly penalizes probabilistic structural models for which there are frequencies at which $\theta^{(1)}(\boldsymbol{h}^{\mathrm{obs}}(\omega_\ell)|\omega_\ell;\boldsymbol{p})$ is small.

6.4 A posteriori error estimation

After the stochastic inverse problem is solved, two methods can be used to evaluate, *a posteriori*, the identified probabilistic structural model. The first method consists in plotting either the sign-reversed loglikelihood or the relative entropy as a function of the frequency as an *a posteriori* error estimate. A plot of this kind indicates the frequencies at which the separation between the experimental data and the identified model is large. The second method consists in comparing the confidence regions predicted by the identified model with either the noise-free observed TFs for an undisturbed vibration test, or with estimates of the noise-free TFs obtained from the noisy observed TFs for a disturbed vibration test. The identified model is then considered invalid at the frequencies for which the (estimates of the) noise-free observed TFs do not lie within the confidence bounds. These two methods are expected to be equivalent, in that the frequencies at which the distance between the experimental data and the identified model is large are expected to coincide with the frequencies for which the (estimates of the) noise-free observed TFs do not lie within the confidence bounds.

On the basis of *a posteriori* error indications of this kind, one can modify if necessary the probabilistic model (for instance, by using a more extensive parameterization), identify the new parameters, and check wether the modified model has led to a reduction of the discrepancies between the experimental data and the identified model.

6.5 Predictive use of the identified model

The identified probabilistic structural model can be used to predict the dynamical behaviour of the complete real structure (i.e. not only at points where experimental data are available). For instance, confidence regions can be built for predicted random TFs. Upon viewing the latter as confidence bounds within which the TFs of the real structure lie, a characterization of the predictive accuracy is obtained: wide confidence intervals mean low predictive accuracy and vice versa. However,

it should be emphasized that the predicted confidence regions do not define hard bounds within which the TFs of the real structure would be guaranteed to lie.

7 Inversion of a probabilistic model of a slender beam

This section presents a comprehensive example of the inversion of a non-parametric probabilistic model using simulated data.

7.1 Problem setting

[Fig. 1 about here.]

The example concerns the dynamical behaviour of the slender beam shown in Figure 1. A right-handed Cartesian reference frame (x_1, x_2, x_3) with origin $\boldsymbol{o}$ is defined. The undeformed beam occupies the box-shaped region

$$\Omega = \Big\{-0.5\,\mathrm{m} < x_1 < 0.5\,\mathrm{m},\ 0 < x_2 < 10\,\mathrm{m},\ 0 < x_3 < 1.5\,\mathrm{m}\Big\}. \tag{59}$$

It is simply supported at $x_2 = 0$ and $x_2 = 10\,\mathrm{m}$. It is constituted of a homogeneous, isotropic, linear elastic material with Young's modulus $E = 33\,\mathrm{GPa}$, Poisson ratio $\nu = 0.3$ and mass density $\rho = 2500\,\mathrm{kg/m^3}$. Its dynamical behaviour is analyzed in the frequency band $B = [0, \omega_{\max}]$, where $\omega_{\max} = 2\pi f_{\max}$ and $f_{\max} = 1000\,\mathrm{Hz}$. Finally, let $\boldsymbol{t}_1$, $\boldsymbol{t}_2$ and $\boldsymbol{t}_3$ denote the points with coordinates $(0,\ 2.5\,\mathrm{m},\ 0.75\,\mathrm{m})$, $(0,\ 5\,\mathrm{m},\ 0.75\,\mathrm{m})$ and $(0,\ 6.4\,\mathrm{m},\ 0.75\,\mathrm{m})$, respectively.

7.2 Simulated data

A data set is synthetically generated with a three-dimensional (3D) FE model constituted of $10 \times 100 \times 15$ isoparametric 8-noded brick elements of equal size. Modal damping is assumed with modal damping ratio $\xi = 0.02$. The beam is loaded by a frequency-dependent pressure $p(\omega)$ uniformly applied on the square portion Γ_p of the top surface centred at $(0.5\,\mathrm{m},\ 4.2\,\mathrm{m},\ 0.75\,\mathrm{m})$ and of area ϵ^2 with $\epsilon \ll 1\,\mathrm{m}$. The vertical response is observed at the points $\boldsymbol{t}_1$, $\boldsymbol{t}_2$ and $\boldsymbol{t}_3$. In the following, we will identify the probabilistic model (to be built) using the response at $\boldsymbol{t}_2$ and $\boldsymbol{t}_3$. The data set $\boldsymbol{D}^{\mathrm{obs}}$ gathers the TFs from the applied pressure field to the vertical response at $\boldsymbol{t}_2$ and $\boldsymbol{t}_3$ predicted by the 3D FE model at the discrete frequencies covering the range between 5 and 1000 Hz with a step of 5 Hz (hence, $n_{\mathrm{M}} = 2$ and $n_{\mathrm{F}} = 200$). We will afterwards use the response at $\boldsymbol{t}_1$ to validate the predictive capability of the identified model.

Deterministic modelling A one-dimensional (1D) FE model made of 100 2-noded Timoshenko beam elements of equal length is built. At the two edges, the translational DOFs are set to zero, while the rotational DOFs are unconstrained. A reduced matrix model of form (7)-(8) is then created using a reduction basis made of n_{T} bending eigenmodes. The j-th diagonal entries of the reduced stiffness, damping and mass matrix are respectively given by $K_{jj} = (w_j^{\mathrm{1D}})^2$, $D_{jj} = 2\xi(w_j^{\mathrm{1D}})$ and $M_{jj} = 1$, where w_j^{1D} is the j-th angular eigenfrequency of the 1D FE model.

Probabilistic modelling A non-parametric probabilistic model is built of form (18)-(19). The mean values of the random reduced matrices are chosen equal to their deterministic counterparts in model (7)-(8), i.e.:

$$E\left\{\mathbb{K}(\boldsymbol{p})\right\} = \boldsymbol{K}\ , \quad E\left\{\mathbb{D}(\boldsymbol{p})\right\} = \boldsymbol{D}\ , \quad E\left\{\mathbb{M}(\boldsymbol{p})\right\} = \boldsymbol{M}. \tag{60}$$

Hence, there are no mean-model parameters, i.e. $\boldsymbol{p}_0 = \emptyset$, and the random matrices $\mathbb{K}(\boldsymbol{p})$, $\mathbb{D}(\boldsymbol{p})$ and $\mathbb{M}(\boldsymbol{p})$ are parameterized solely by their respective dispersion parameters δ_{K}, δ_{D} and δ_{M}. For the sake of simplicity, it is assumed that $\delta_{\mathrm{K}} = \delta_{\mathrm{D}} = \delta_{\mathrm{M}} = \delta$, so that $\boldsymbol{p} = \{\delta\}$ is the only active parameter of the probabilistic model.

Random matrix eigenvalue problem

[Fig. 2 about here.]

Before studying in the next section the stochastic properties of the random TFs predicted by the probabilistic model, the present section analyzes the random matrix eigenvalue problem (App. A) defined by the random reduced stiffness and mass matrices $\mathbb{K}(\boldsymbol{p})$ and $\mathbb{M}(\boldsymbol{p})$. Since the stochastic properties of the predicted random TFs are strongly related to the properties of the random eigenfrequencies and eigenmodes defined by these random matrices, the analysis of the latter provides useful insight into the former. The random eigenfrequencies are now studied for frequencies lower than $1.5 \times f_{\max} = 1500\,\mathrm{Hz}$.

First, the stochastic properties of the eigenfrequencies as a function of the dimension n_{T} of the reduction basis are studied. Figure 2(a) shows the 50 lowest deterministic eigenfrequencies of the mean model, and the mean value (computed using $n_{\mathrm{S}} = 10000$ Monte Carlo simulations) of the random eigenfrequencies for δ=0.8 and $n_{\mathrm{T}} = 20,\ 30,\ 40$ and 50. Since the eigenfrequencies are non-linear functions of the stiffness and mass matrices, their mean value differs from the deterministic eigenfrequencies. For a fixed n_{T}, the mean values of the low eigenfrequencies (approximately the lowest $n_{\mathrm{T}}/2$) are observed to be smaller than the deterministic values, while the mean values of the high eigenfrequencies are observed to be larger. For the

eigenfrequencies lower than 1000 Hz, reasonable convergence is obtained for $n_{\mathrm{T}} = 50$. All results to follow have been obtained with $n_{\mathrm{T}} = 50$ eigenmodes.

Figure 2(b) shows the PDFs (computed using $n_{\mathrm{S}} = 10000$ Monte Carlo simulations) of the random eigenfrequencies for $\delta = 0.2$ and $\delta = 0.8$ in the frequency range up to 1000 Hz. For $\delta = 0.2$, the dispersion of the random eigenfrequencies is small compared to the eigenfrequency separation and the PDFs do not overlap. For $\delta = 0.8$, the dispersion of the random eigenfrequencies is large compared to the eigenfrequency separation and the PDFs do overlap except for the 3 lowest eigenfrequencies. Furthermore, these random eigenfrequencies are observed to decrease as δ increases.

Predicted random TFs

[Fig. 3 about here.]

Figure 3 shows, as a function of the number n_{S} of Monte Carlo simulations, the statistical mean of the realizations of the predicted random TF at $\boldsymbol{t}_2$ for the dispersion levels $\delta = 0.2$ and $\delta = 0.8$ at the frequencies 200 Hz and 800 Hz. The larger δ and the higher the frequency, the larger the required number n_{S} becomes. Fully converged results are clearly obtained for $n_{\mathrm{S}} = 10000$. All results to follow have been obtained using $n_{\mathrm{S}} = 10000$ Monte Carlo simulations.

[Fig. 4 about here.]

Figure 4 shows the 99%-confidence regions for the predicted random TF at $\boldsymbol{t}_2$ and $\boldsymbol{t}_3$ for $\delta = 0.2$ and $\delta = 0.8$. Their width is observed to increase with δ and also with the frequency, highlighting that the predictions become more sensitive to uncertainties as the frequency increases. At low frequencies below approximately 200 Hz, the frequencies of the resonance peaks are observed to decrease when δ increases. On the other hand, at frequencies above 200 Hz, the confidence bounds for $\delta = 0.2$ show resonance peaks while the confidence bounds for $\delta = 0.8$ do not. Indeed, for $\delta = 0.2$, the dispersion of the random eigenfrequencies is small compared to the eigenfrequency separation resulting in resonances randomly occurring in distinct frequency ranges. In contrast, for $\delta = 0.8$, the dispersion is large compared to the separation, so that resonances randomly occur at all frequencies.

7.4 Stochastic inverse problem

Identification of the probabilistic model

[Fig. 5 about here.]

The suitable dispersion level is identified by minimizing the distance $\mathcal{L}$, defined in (28). Figure 5 shows that the probabilistic model with the largest admissible dispersion level $\hat{\delta} = 0.96$, with reference to inequality (17), is optimal.

A posteriori error estimation

[Fig. 6 about here.]

Figure 6(a) shows the sign-reversed loglikelihood of $\hat{\delta} = 0.96$ as a function of the frequency. Figures 6(b) and 6(c) compare the 99%-confidence regions for the identified predicted random TFs to the observed TFs at $\boldsymbol{t}_2$ and $\boldsymbol{t}_3$. The sign-reversed loglikelihood is seen to be large at frequencies for which the observed TFs do not lie within the confidence bounds. At low frequencies below 200 Hz, the agreement of the identified model with the data is unsatisfactory. Due to the decrease of the low random eigenfrequencies with δ, the low-frequency resonances of the random TFs are located at lower frequencies than those of the observed TFs.

Modification of the probabilistic model To mitigate the discrepancy at the low frequencies, the probabilistic model is modified. The non-parametric probabilistic model used in the following has the same form (18)-(19), but, this time, the mean values of the random reduced stiffness and damping matrices are defined by:

$$E\left\{\mathbb{K}(\boldsymbol{p})\right\} = \boldsymbol{K}(w_1, w_2, w_3) \ , \quad E\left\{\mathbb{D}(\boldsymbol{p})\right\} = \boldsymbol{D}(w_1, w_2, w_3) \quad , \tag{61}$$

with:

$$\begin{array}{ll} K_{jj}(w_1, w_2, w_3) = w_j^2 \ , & D_{jj}(w_1, w_2, w_3) = 2\xi w_j \quad (j = 1, 2, 3) \quad , \\ K_{jj}(w_1, w_2, w_3) = (w_j^{\mathrm{1D}})^2 \ , & D_{jj}(w_1, w_2, w_3) = 2\xi w_j^{\mathrm{1D}} \quad (4 \leq j \leq n_{\mathrm{T}}). \end{array}$$

The three lowest angular eigenfrequencies w_1, w_2 and w_3 are now used as mean-model parameters. The mean value of the random reduced mass matrix is still defined by (60). The three dispersion parameters are again chosen equal: $\boldsymbol{p}_\delta = \{\delta\}$, such that now $\boldsymbol{p} = \{w_1, w_2, w_3, \delta\}$.

Identification of the modified probabilistic model The distance $\mathcal{L}(\boldsymbol{p})$ is minimized by the parameters $\hat{w}_1/2\pi = 46.67$ Hz, $\hat{w}_2/2\pi = 172.63$ Hz, $\hat{w}_3/2\pi = 230.00$ Hz and $\hat{\delta} = 0.67$.

A posteriori error estimation

[Fig. 7 about here.]

Figure 7(a) shows the sign-reversed loglikelihood of $\hat{w}_1/2\pi = 46.67\,\text{Hz}$, $\hat{w}_2/2\pi = 172.63\,\text{Hz}$, $\hat{w}_3/2\pi = 230.00\,\text{Hz}$ and $\hat{\delta} = 0.67$ as a function of the frequency. Figures 7(b) and 7(c) compare the 99%-confidence regions for the identified predicted random TFs to the observed TFs at $\boldsymbol{t}_2$ and $\boldsymbol{t}_3$. Compared to Figure 6(a), the sign-reversed loglikelihood has been reduced at the low frequencies. The observed TFs are seen to lie within the confidence bounds at all frequencies. The introduction of the mean-model parameters has allowed to compensate for the decrease of the lowest random eigenfrequencies.

Predictive use of the identified probabilistic model

[Fig. 8 about here.]

To validate the predictive capability of the identified probabilistic model, Figure 8 compares the 99%-confidence region for the random TF predicted by the identified probabilistic model at the point $\boldsymbol{t}_1$ to the corresponding TF predicted by the 3D FE model. The latter TF is seen to lie within the confidence bounds at all frequencies. This result suggests that the identified model can be used in a predictive manner, namely to predict the dynamical behaviour of the slender beam at points where no observed TFs are available.

8 Inversion of a probabilistic model for ground-borne vibrations in buildings

This section presents a civil and environmental engineering case history involving the inversion of a non-parametric probabilistic model from real experimental data.

8.1 Problem setting

[Fig. 9 about here.]

The case history concerns the transmission of vibrations from the underground-railway tunnel of the RER B line of RATP to the Maison du Mexique building at the Cité Universitaire site in Paris in France (Fig. 9). The tunnel is a masonry cut-and-cover tunnel at a shallow depth of about 9.3 m below the free surface of the soil embedded in sand layers. Two classic ballast tracks are running in the tunnel. The Maison du Mexique is a six-storey reinforced-concrete frame structure. It has two sets of eight columns such that the floor spans are approximately 6.2 m. The floor-to-ceiling height is approximately 2.85 m.

[Fig. 10 about here.]

For the tunnel, a right-handed Cartesian frame of reference $(\boldsymbol{i}'_1, \boldsymbol{i}'_2, \boldsymbol{i}'_3)$ is defined with the origin $\boldsymbol{o}'$ at the free surface of the soil (Fig. 10). For the building, a right-handed Cartesian frame of reference $(\boldsymbol{i}_1, \boldsymbol{i}_2, \boldsymbol{i}_3)$ is defined with the origin $\boldsymbol{o}$ in the left corner at the ground floor (Fig. 10). The origin of the reference frame of the building has coordinates $(x'_1 = -23.5\,\mathrm{m},\ x_2 = -24.3\,\mathrm{m},\ x_3 = 0)$ in the reference frame of the tunnel. The angle between $\boldsymbol{i}_2$ and $\boldsymbol{i}'_2$ is 25°.

8.2 Real experimental data

[Fig. 11 about here.]

In the frame of the European CONVURT project (the CONtrol of Vibrations from Underground Railway Traffic), *in situ* measurements were performed of the dynamical response in the Maison du Mexique due to excitations applied on the rails in the tunnel. Vibrations were generated by an impact of an instrumented hammer with a mass of 5.3 kg and a soft tip on the rail head at the point with coordinates $(x'_1 = -2.5\,\mathrm{m},\ x'_2 = 0,\ x'_3 = -8.2\,\mathrm{m})$, and recorded by accelerometers placed at different locations in the Maison du Mexique. We will consider here the vertical response at the locations BA01, F0PL and F201 (Fig. 11 and Table A.1).

[Table 1 about here.]

[Fig. 12 about here.]

A total of $n_\mathrm{R} = 25$ events was recorded. The A/D conversion was performed at a rate of 1000 Hz. A total of 4096 data points was recorded for each event (hence, the frequency-domain resolution is 0.2441 Hz). Estimates of the noise-free TFs from the force applied on the rail head to the vertical velocity in the building have been deduced from the noisy experimental data using the $H1$-estimation method. Figure 12 shows the time history of the response measured during the sixth event, the estimated noise-free TF and the coherence function at BA01, F0PL and F201. Due to experimental noise, low coherence values, indicating low data quality, are observed at frequencies below 20 Hz and at frequencies above 100 Hz. The coherence decreases with the distance to the impact point.

In the following, we will identify the probabilistic model (to be built) using the TFs at BA01 and F0PL. The data set $\tilde{\boldsymbol{D}}^{\mathrm{obs}}$ gathers the observed TFs from the applied force to the response at BA01 and F0PL at the discrete frequencies covering the range between 20 and 100 Hz with a step of 0.2441 Hz (hence, $n_\mathrm{M} = 2$ and $n_\mathrm{F} = 327$). We will afterwards use the vertical response at the measurement location F201 to validate the predictive capability of the identified model.

Deterministic modelling On the basis of the assumption that the dynamic interaction of the track, the tunnel and the soil is only weakly coupled to the dynamic interaction of the soil and the building, the transmission of the vibrations is modelled in two steps. First, a model for the dynamical interaction of the track, the tunnel and the soil is used to compute the wave field radiated into the soil due to forces applied on the rails in the tunnel. The dynamic track-tunnel-soil interaction model is based on the periodic coupled Finite Element-Boundary Element (FE-BE) formulation proposed by Clouteau et al. [61]. Subsequently, a model for the dynamic interaction of the soil and the building is used to compute the structural vibration induced by this incident wave field. The dynamic soil-building interaction model uses a classical coupled FE-BE formulation in conjunction with the Craig-Bampton substructuring method, see e.g. [62].

The reduced matrix model for the groundborne vibrations in the Maison du Mexique thus obtained has the following form [63]:

$$[\boldsymbol{K} + i\omega\boldsymbol{D} - \omega^2\boldsymbol{M} + \boldsymbol{K}_{\mathrm{S}}(\omega)]\boldsymbol{q}(\omega) = \boldsymbol{f}_{\mathrm{S}}(\omega)\ , \quad \omega \in B \quad , \tag{62}$$

$$\boldsymbol{u}(\omega) = \boldsymbol{T}\boldsymbol{q}(\omega). \tag{63}$$

The matrices $\boldsymbol{K}$, $\boldsymbol{D}$ and $\boldsymbol{M}$ are the reduced stiffness, damping and mass matrices of the building. For a fixed frequency ω, the matrix $\boldsymbol{K}_{\mathrm{S}}(\omega)$ is the dynamic soil impedance matrix, $\boldsymbol{f}_{\mathrm{S}}(\omega)$ is the vector of the generalized forces (the virtual work on the soil-building-interface modes generated by the tractions induced by the incident wave field on a fixed foundation), $\boldsymbol{q}(\omega)$ is the vector of the generalized coordinates and $\boldsymbol{u}(\omega)$ collects the FE DOFs of the building. The rectangular matrix $\boldsymbol{T}$ is the transformation matrix of the reduction basis.

Probabilistic modelling A non-parametric probabilistic model, associated to the deterministic model (64)-(65), is built:

$$[\mathbb{K}(\boldsymbol{p}) + i\omega\mathbb{D}(\boldsymbol{p}) - \omega^2\mathbb{M}(\boldsymbol{p}) + \boldsymbol{K}_{\mathrm{S}}(\omega)]\mathbb{Q}(\omega;\boldsymbol{p}) = \boldsymbol{f}_{\mathrm{S}}(\omega)\ , \quad \omega \in B \quad , \tag{64}$$

$$\mathbb{U}(\omega;\boldsymbol{p}) = \boldsymbol{T}\mathbb{Q}(\omega;\boldsymbol{p}). \tag{65}$$

The reduced stiffness, damping and mass matrices of the building are modelled by the random matrices $\mathbb{K}(\boldsymbol{p})$, $\mathbb{D}(\boldsymbol{p})$ and $\mathbb{M}(\boldsymbol{p})$, respectively, parameterized by $\boldsymbol{p}$. The dynamic soil impedance matrix and the vector of the generalized forces are kept deterministic.

The mean values of the random reduced matrices are chosen equal to their deterministic counterparts in model (64)-(65). Hence, there are no mean-model parameters, i.e. $\boldsymbol{p}_0 = \emptyset$, and the random matrices $\mathbb{K}(\boldsymbol{p})$, $\mathbb{D}(\boldsymbol{p})$ and $\mathbb{M}(\boldsymbol{p})$ are parameterized solely by their respective dispersion parameters δ_{K}, δ_{D} and δ_{M}. For the sake of simplicity,

it is assumed that $\delta_K = \delta_D = \delta_M = \delta$, such that $\boldsymbol{p} = \{\delta\}$ is the only active parameter of the probabilistic model.

Predicted random TFs

[Fig. 13 about here.]

The predicted random TFs are obtained in two steps. First, the deterministic dynamic track-tunnel-soil interaction model is used to compute the wave field radiated by the tunnel into the soil due to the application of a unitary vertical excitation on the rail head at the point with coordinates ($x'_1 = -2.5\,\mathrm{m},\ x'_2 = 0,\ x'_3 = -8.2\,\mathrm{m}$). Subsequently, the probabilistic model (64)-(65) is used to compute the random building response due to this incident wave field.

Figure 13 shows, as a function of the number n_S of Monte Carlo simulations, the statistical mean of the realizations of the predicted random TF at F0PL for the dispersion levels $\delta = 0.2$ and $\delta = 0.8$ at the frequencies 50 Hz and 100 Hz. Reasonably converged results are obtained for $n_S = 400$, and this value is used for all subsequent computations.

[Fig. 14 about here.]

Figure 14 shows the 99%-confidence regions for the predicted random TFs at BA01 and F0PL for $\delta = 0.2$ and $\delta = 0.8$. Their width is observed to increase with δ and also with the frequency, highlighting that the predictions become more sensitive to uncertainties as the frequency increases. At the floor slabs of the building, where the response is governed by clusters of local plate bending modes [63], the confidence regions are very wide, even for small values of δ.

8.4 Stochastic inverse problem

Identification of the probabilistic model

[Fig. 15 about here.]

Figure 15 shows the distances $\mathcal{L}(\delta)$ and $\mathcal{J}(\delta)$ as a function of the dispersion level δ. The probabilistic structural model with the dispersion level $\hat{\delta} = 0.8$ is seen to be optimal for both distances.

***A posteriori* error estimation**

[Fig. 16 about here.]

Figure 16(a) shows the sign-reversed loglikelihood of, and the relative entropy for, $\hat{\delta} = 0.8$ as a function of the frequency. Figures 16(b) and 16(c) compare the 99%-confidence region for the identified predicted random TF to the estimate of the noise-free TF at BA01 and F0PL. At the frequencies for which the coherence function is large (Fig. 12), the sign-reversed loglikelihood and the relative entropy are large whenever the estimates of the noise-free TFs do not lie within the confidence bounds. At frequencies between about 20 and 30 Hz, the agreement of the identified model with the data is unsatisfactory at BA01. This discrepancy can be traced back to the dynamic track-tunnel-soil interaction model, in that an energy loss occurs in the computed incident wave field at these frequencies. A first possible step that could be taken to mitigate this discrepancy is to modify the dynamic track-tunnel-soil interaction model so as to bring the computed incident wave field into agreement with the experimental data. Another possibility is to introduce uncertainty in the incident wave field, or, equivalently, in the vector of the generalized forces in (64)-(65). Such modifications are not addressed in this article and are left as a direction for future work.

Predictive use of the identified probabilistic model

[Fig. 17 about here.]

Figure 17 compares the 99%-confidence region for the random TF predicted by the identified probabilistic model to the estimate of the noise-free TF at F201. At the frequencies for which the coherence function is large (Fig. 12), the estimate of the noise-free TF is seen to lie within the confidence bounds. It should be noted that this result is not fully conclusive on the predictive capability of the identified model since the measured response at F201 is very noisy.

9 Conclusions and directions for future work

This article addressed the inversion of probabilistic structural models using measured TFs. We worked with probabilistic structural models with minimal parameterization. Their first interest is that they fulfil, by construction, the essential mathematical and physical properties of probabilistic structural models. Since they depend on only a small set of parameters, their second advantage is that their inversion can generally be formulated as a mathematically well-posed inverse problem that is numerically solvable with a reasonable computational effort. We first showed that the method of maximum likelihood is not well-adapted to the inversion of probabilistic structural models using measured TFs, due to computational difficulties and model incompatibility. We then formulated the inversion of probabilistic models alternatively as the minimization of an objective function that measures a distance

between the experimental data and the probabilistic model. Two principles of construction for the definition of such distances were proposed, based either upon the loglikelihood function, or the relative entropy. We showed that the use of distances accounting only for first-order cylindrical PDFs allows circumventing the aforementioned difficulties.

The proposed methodology was demonstrated on examples featuring successively simulated and real experimental data. The first example highlighted that it may sometimes be useful to parameterize non-parametric probabilistic models with minimal parameterization by mean-model parameters. Indeed, the low-frequency random eigenfrequencies of probabilistic models of this kind were found to decrease as the dispersion level increases. If a large dispersion level is required, the introduction of mean-model parameters allows to compensate for this decrease. The mean-model parameters must clearly be identified together with the dispersion parameters. In the second example, the inverse methods based on the minimization of the distances $\mathcal{L}$ and $\mathcal{J}$ were found to lead to similar results in that, in that particular example, the same dispersion level was found to be optimal in the sense of the two distances.

In both examples, the simplifying assumption was made that the dispersion levels of the stiffness, damping and mass matrix are identical. A natural direction for future work consists in relaxing this assumption. Furthermore, in the second example, the soil impedance matrix was kept deterministic. The probabilistic modelling of the impedance matrix [64] is a second direction for future work.

Finally, it is noted that the inverse methods proposed in this article are not limited in scope to the identification of probabilistic models with minimal parameterization, and can also be applied to cases in which the probabilistic model depends on a large number of parameters, for instance the coefficients of a polynomial chaos expansion. However, the stochastic inverse problems thus obtained may be mathematically ill-posed, and the issue of their regularization arises, e.g. by means of Tikhonov or Bayesian approaches [65].

Acknowledgements

The results presented in this paper were obtained in the frame of a BDI scholarship provided by the CNRS. The second illustration is based on results obtained in the frame of the EC-Growth project G3RD-CT-2000-00381 CONVURT ("The CONtrol of Vibration from Underground Railway Traffic"). The financial support of the CNRS and of the European Community is gratefully acknowledged.

A Random matrix eigenvalue problem

In this appendix, a random matrix eigenvalue problem is formulated using the random reduced structural matrices introduced in Section 3.2. We note that considerable effort has already been expended in the literature to the study of random matrix eigenvalue problems, see e.g. [66, 67].

Let $\boldsymbol{K}, \boldsymbol{M} \in \mathrm{M}^+_{n_\mathrm{T}}(\mathbb{R})$ be reduced stiffness and mass matrices obtained by the projection of corresponding FE stiffness and mass matrices onto a reduction basis. Let the random matrices $\mathbb{K}$ and $\mathbb{M}$, defined on $(\mathcal{A}, \mathcal{T}, P)$, be corresponding random reduced stiffness and mass matrices such that:

$$\mathbb{K} = \boldsymbol{L}_\mathrm{K}^\mathrm{T} \mathbb{N}_\mathrm{K} \boldsymbol{L}_\mathrm{K} \ , \quad \mathbb{M} = \boldsymbol{L}_\mathrm{M}^\mathrm{T} \mathbb{N}_\mathrm{M} \boldsymbol{L}_\mathrm{M} \quad , \tag{A.1}$$

where $\mathbb{N}_\mathrm{K}$ and $\mathbb{N}_\mathrm{M}$ are normalized random matrices, and $\boldsymbol{L}_\mathrm{K}$ and $\boldsymbol{L}_\mathrm{M}$ are the Cholesky factors of $\boldsymbol{K}$ and $\boldsymbol{M}$, respectively. Since $\mathbb{N}_\mathrm{K}$ and $\mathbb{N}_\mathrm{M}$ are normalized matrices, we have:

$$E\left\{\mathbb{K}\right\} = \boldsymbol{K} \ , \quad E\left\{\mathbb{M}\right\} = \boldsymbol{M}. \tag{A.2}$$

The random matrices $\mathbb{K}$ and $\mathbb{M}$ define the following random matrix eigenvalue problem:

$$\mathbb{K}\mathbb{Q}_k = \mathbb{W}_k^2 \mathbb{M}\mathbb{Q}_k \quad , \tag{A.3}$$

where the collection $\{\mathbb{Q}_k \mid 1 \leq k \leq n_\mathrm{T}\}$ gathers the random eigenvectors and $\{\mathbb{W}_k \mid 1 \leq k \leq n_\mathrm{T}\}$ collects the random circular eigenfrequencies.

Since the eigenfrequencies are non-linear functions of the reduced matrices, the mean values of the random eigenfrequencies generally differ from the eigenfrequencies of the mean matrices $\boldsymbol{K}$ and $\boldsymbol{M}$. The lowest, and the highest, random eigenfrequencies are generally smaller, and larger, than the corresponding eigenfrequencies of the mean matrices. This can be understood from the Rayleigh quotient. For a fixed $a \in \mathcal{A}$, the realizations $\{\mathbb{W}_k(a) \mid 1 \leq k \leq n_\mathrm{T}\}$ associated to the realizations $\mathbb{K}(a)$ and $\mathbb{M}(a)$ can be obtained by the sequential minimization of the Rayleigh quotient, see e.g. [68]:

$$\mathbb{W}_k^2(a) = \arg \min_{\boldsymbol{x} \in \mathcal{W}_k(a)} \frac{\boldsymbol{x}^\mathrm{T} \mathbb{K}(a) \boldsymbol{x}}{\boldsymbol{x}^\mathrm{T} \mathbb{M}(a) \boldsymbol{x}} \quad , \tag{A.4}$$

where $\mathcal{W}_k(a)$ is the subspace of $\mathbb{R}^{n_\mathrm{T}}$ orthogonal to the eigenvectors with lower eigenfrequencies. The sequential minimization first finds the vectors $\boldsymbol{x}$ combining a smaller elastic energy $\boldsymbol{x}^\mathrm{T}\mathbb{K}(a)\boldsymbol{x} < \boldsymbol{x}^\mathrm{T}\boldsymbol{K}\boldsymbol{x}$ with a larger kinetic energy $\boldsymbol{x}^\mathrm{T}\mathbb{M}(a)\boldsymbol{x} > \boldsymbol{x}^\mathrm{T}\boldsymbol{M}\boldsymbol{x}$ such that the lowest random eigenfrequencies (and their mean values) are generally smaller than the corresponding eigenfrequencies of $\boldsymbol{K}$ and $\boldsymbol{M}$. In contrast, at the end of the sequential minimization process, the space $\mathcal{W}_k(a)$ spans vectors $\boldsymbol{x}$ with $\boldsymbol{x}^\mathrm{T}\mathbb{K}(a)\boldsymbol{x} > \boldsymbol{x}^\mathrm{T}\boldsymbol{K}\boldsymbol{x}$ and $\boldsymbol{x}^\mathrm{T}\mathbb{M}(a)\boldsymbol{x} < \boldsymbol{x}^\mathrm{T}\boldsymbol{M}\boldsymbol{x}$ such that the highest random eigenfrequencies (and their mean values) are generally larger the corresponding eigenfrequencies of $\boldsymbol{K}$ and $\boldsymbol{M}$.

References

[1] M.J. Friswell and J.E. Mottershead. *Finite element model updating in structural dynamics*. Kluwer, Dordrecht, The Netherlands, 1995.

[2] L. Ljung. *System Identification: Theory for the User*. Prentice Hall PTR, 1987.

[3] R. Pintelon and J. Schoukens. *System Identification: a Frequency Domain Approach*. Wiley-IEEE Press, 2001.

[4] E. Savin. Midfrequency vibrations of a complex structure: experiments and comparison with numerical simulations. *AIAA Journal*, 40:1876–1884, 2002.

[5] R.A. Ibrahim. Structural dynamics with parameter uncertainties. *ASME Applied Mechanics Reviews*, 40:309–328, 1987.

[6] C.S. Manohar and R.A. Ibrahim. Progress in structural dynamics with stochastic parameter variations 1987-1998. *ASME Applied Mechanics Reviews*, 52: 177–197, 1999.

[7] G.I. Schueller, L.A. Bergman, C.G. Bucher, G. Dasgupta, G. Deotdatis, R.G. Ghanem, M. Grigoriu, M. Hoshiya, E.A. Johnson, N.A. Naess, H.J. Pradlwarter, M. Shinozuka, K. Sobszyck, P.D. Spanos, B.F. Spencer, A. Sutoh, T. Takada, W.V. Wedig, S.F. Wojtkiewicz, I. Yoshida, B.A. Zeldin, and R. Zhang. A state-of-the-art report on computational stochastic mechanics. *Probabilistic Engineering Mechanics*, 12:197–321, 1997.

[8] G.I. Schueller. Computational stochastic mechanics - recent advances. *Computers and Structures*, 79:2225–2234, 2001.

[9] R. Ghanem and P. Spanos. *Stochastic Finite Elements:A Spectral Approach*. Springer, 1991.

[10] Y.K. Lin and G.Q. Cai. *Probabilistic Structural Dynamics*. McGraw-Hill, 1995.

[11] C. Soize. A non-parametric model of random uncertainties for reduced matrix models in structural dynamics. *Probabilistic Engineering Mechanics*, 15:277–294, 2000.

[12] C. Soize. Maximum entropy approach for modeling random uncertainties in transient elastodynamics. *Journal of the Acoustical Society of America*, 109: 1979–1996, 2001.

[13] C. Desceliers, R. Ghanem, and C. Soize. Maximum likelihood estimation of stochastic chaos representations from experimental data. *International Journal for Numerical Methods in Engineering*, 66:978–1001, 2006.

[14] C. Soize and R. Ghanem. Physical systems with random uncertainties: chaos representations with arbitrary probability measure. *SIAM Journal on Scientific Computing*, 26:395–410, 2004.

[15] N. Wiener. The homogeneous chaos. *Americal Journal of Mathematics*, 60: 897–936, 1938.

[16] C. Soize. Non-Gaussian positive-definite matrix-valued random fields for elliptic stochastic partial differential operators. *Computer Methods in Applied Mechanics and Engineering*, 195:26–64, 2006.

[17] C. Shannon. A mathematical theory of communications. *Bell Systems Technical Journal*, 27:379–423, 1948.

[18] E.T. Jaynes. Information theory and statistical mechanics. *Physical Review*,

106:620–630, 1957.
[19] E.T. Jaynes. *Probability theory: The Logic of Science*. Cambridge University Press, 2003.
[20] E. Balmès. Frequency domain identification of structural dynamics using the pole/residue parametrization. In *International Modal Analysis Conference*, Dearborn, USA, 1996.
[21] G. Casella and R.L. Berger. *Statistical Inference*. Duxbury Press, 2001.
[22] S. Kullback. *Information Theory and Statistics*. Dover Publications, 1968.
[23] E.L. Lehmann and G. Casella. *Theory of Point Estimation*. Springer, 1998.
[24] H. Cramér. *Mathematical Methods of Statistics*. Princeton University Press, 1946.
[25] A. Stuart, K. Ord, and S. Arnold. *Kendall's Advanced Theory of Statistics, Volume 2A: Classical Inference and the Linear Model*. Arnold Hodder, 1999.
[26] A. O'Hagan and J. Forster. *Kendall's Advanced Theory of Statistics, Volume 2B: Bayesian Inference*. Arnold Hodder, 2004.
[27] C. Soize. Random matrix theory for modeling uncertainties in computational mechanics. *Computer Methods in Applied Mechanics and Engineering*, 194: 1333–1366, 2005.
[28] E. Capiez-Lernout. *Dynamique des structures tournantes à symétrie cyclique en présence d'incertitudes aléatoires. Application au désaccordage des roues aubagées*. PhD thesis, Université de Marne-La-Vallée, France, 2004.
[29] C. Chen, D. Duhamel, and C. Soize. Probabilistic approach for model and data uncertainties and its experimental identification in structural dynamics: Case of composite sandwich panels. *Journal of Sound and Vibration*, 294:64–81, 2006.
[30] C. Desceliers, C. Soize, and R.G. Ghanem. Identification of chaos representations of elastic properties of random media using experimental vibration tests. *Computational Mechanics*, 2006. In Press.
[31] R.G. Ghanem and A. Doostan. On the construction and analysis of stochastic models: Characterization and propagation of the errors associated with limited data. *Journal of Computational Physics*, 217:63–81, 2006.
[32] L. Ljung. Some results on identifying linear systems using frequency domain data. In *Proceedings of the 32nd IEEE Conference on Decision and Control*, pages 3534–3538, San Antonio, USA, 1993.
[33] J.L. Beck and L.S. Katafygiotis. Updating models and their uncertainties I: Bayesian statistical framework. *Journal of Engineering Mechanics*, 124:455–461, 1998.
[34] K.-V. Yuen and L.S. Katafygiotis. Bayesian modal updating using complete input and incomplete response noisy measurements. *Journal of Engineering Mechanics*, 128:340–350, 2002.
[35] G.C. Goodwin, M. Gevers, and B. Ninness. Quantifying the error in estimated transfer functions with application to model order selection. *IEEE Transactions on Automatic Control*, 37:913–928, 1992.
[36] W. Reinelt, A. Garulli, and L. Ljung. Comparing different approaches to model error modelling in robust identification. *Automatica*, 38:787–803, 2002.
[37] C. Soize. A comprehensive overview of non-parametric probabilistic approach

of random uncertainties for predictive models in structural dynamics. *Journal of Sound and Vibration*, 288:623–652, 2005.

[38] L.A. Chernov. *Wave Propagation in a Random Medium*. Dover Publications, 1968.

[39] Y.A. Kravtsov, A. Kasilar, S.A. Shapiro, S. Buske, and T. Müller. Estimating statistical parameters of an elastic random medium from traveltime fluctuations of refracted waves. *Waves in Random and Complex Media*, 15:43–60, 2005.

[40] B. Iooss. Seismic reflection traveltimes in two-dimensional statistically anisotropic random media. *Geophysical Journal International*, 135:999–1010, 1998.

[41] S. Kullback and R.A. Leibler. On information and sufficiency. *Annals of Mathematical Statistics*, 22:79–86, 1951.

[42] J.N. Kapur and H.K. Kesavan. *Entropy optimisation principles with applications*. Academic Press, San Diego, 1992.

[43] R. Ohayon and C. Soize. *Structural Acoustics and Vibration*. Academic Press, 1998.

[44] C. Soize. Reduced models in the medium frequency range for general dissipative structural-dynamics systems. *European Journal of Mechanics, A:Solids*, 17: 657–685, 1998.

[45] A. Sarkar and R. Ghanem. Mid-Frequency structural dynamics with parameter uncertainty. *Computer Methods in Applied Mechanics and Engineering*, 191: 5499–5513, 2002.

[46] R.A. Fisher. On the mathematical foundations of theoretical statistics. *Philosophical Transactions of the Royal Society A*, 222:309–368, 1922.

[47] I. Csiszár. Information type measures of difference of probability distributions and indirect observations. *Studia Scientiarum Mathematicarum Hungarica*, 2: 299–318, 1967.

[48] D.W. Scott. *Multivariate Density Estimation: Theory, Practice, and Visualization*. Wiley-Interscience, 1992.

[49] J. Besag. Spatial interaction and the statistical analysis of lattice systems. *Journal of the Royal Statistical Society B*, 36:192–236, 1974.

[50] J. Besag. Statistical analysis of non-lattice data. *The Statistician*, 24:179–195, 1975.

[51] D.J. Nott and T. Ryden. Pairwise likelihood methods for inference in image models. *Biometrika*, 86:661–676, 1999.

[52] D.R. Cox and N. Reid. A note on pseudolikelihood constructed from marginal densities. *Biometrika*, 91:729–737, 2004.

[53] B.G. Lindsay. Composite likelihood methods. In N.U. Prabhu, editor, *Statistical Inference from Stochastic Processes*, pages 221–239. Americal Mathematical Society, 1998.

[54] E. Parzen. On estimation of probability density function and mode. *Annals of Mathematical Statistics*, 33:1065–1076, 1962.

[55] M. Rosenblatt. Remarks on some nonparametric estimates of a density function. *Annals of Mathematical Statistics*, 27:832–837, 1956.

[56] C.P. Robert and G. Casella. *Monte Carlo Statistical Methods*. Springer, 2005.

[57] S. Kirkpatrick, C.D. Gelatt, and M.P. Vecchi. Optimization by simulated annealing. *Science*, 220:671–680, 1983.

[58] N. Metropolis, A.W. Rosenbluth, M.N. Rosenbluth, A.H. Teller, and E. Teller. Equations of state calculations by fast computing machines. *The Journal of Chemical Physics*, 21:1087–1092, 1953.

[59] D.E. Goldberg. *Genetic Algorithms in Search, Optimization and Machine Learning.* Addison-Wesley Professional, 1989.

[60] D.B. Fogel. *Evolutionary Computation : Towards a New Philosophy of Machine Intelligence.* IEEE Computer Society Press, 1995.

[61] D. Clouteau, M. Arnst, T.M. Al Hussaini, and G. Degrande. Free field vibrations due to dynamic loadings on a tunnel embedded in a stratified medium. *Journal of Sound and Vibration*, 283:173–199, 2005.

[62] D. Clouteau and D. Aubry. A subdomain approach to dynamic soil-structure interaction. In W.S. Hall and G. Oliveto, editors, *Boundary Element Methods for Soil-Structure Interaction*, pages 61–125. Springer, 2003.

[63] M. Arnst, D. Clouteau, H. Chebli, R. Othman, and G. Degrande. A nonparametric probabilistic model for ground-borne vibrations in buildings. *Probabilistic Engineering Mechanics*, 21:18–34, 2006.

[64] R. Cottereau. *Probabilistic models of impedance matrices. Application to dynamic soil-structure interaction.* PhD thesis, École Centrale Paris, France, 2007.

[65] A. Tarantola. *Inverse Problem Theory and Methods for Model Parameter Estimation.* SIAM, 2005.

[66] S. Adhikari. Random matrix eigenvalue problems in structural dynamics. *International Journal for Numerical Methods in Engineering*, 69:562–591, 2007.

[67] S. Rahman. A solution of the random eigenvalue problem by a dimensional decomposition method. *International Journal for Numerical Methods in Engineering*, 67:1318–1340, 2006.

[68] M. Géradin and D. Rixen. *Mechanical Vibrations : Theory and Applications to Structural Dynamics.* John Wiley & Sons, 1992.

List of Figures

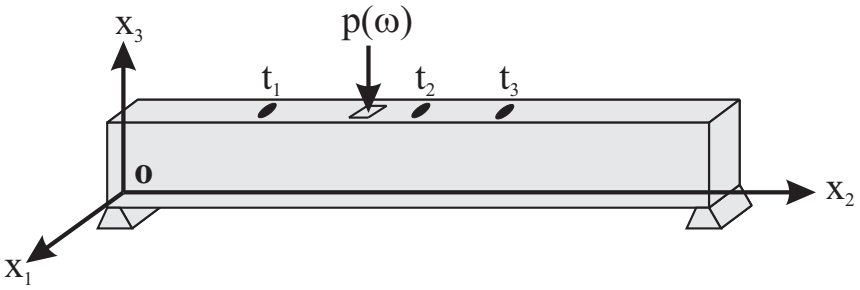

Fig. 1. Slender beam: schematic representation.

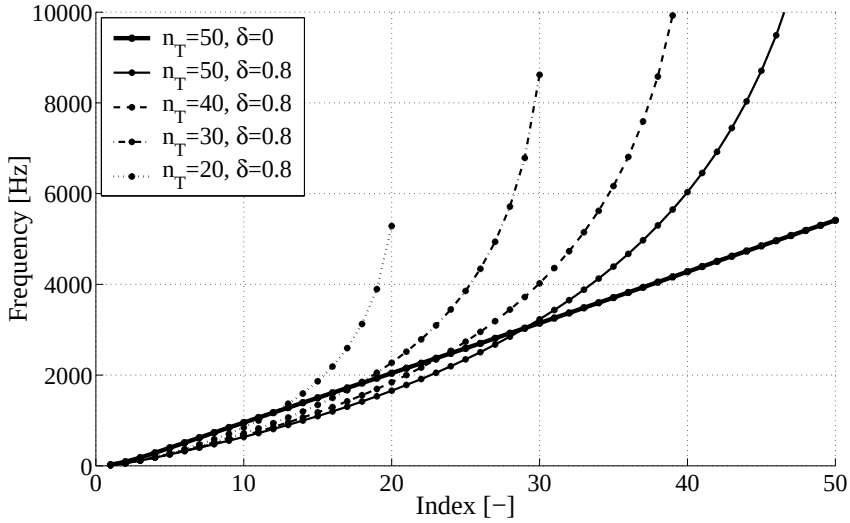

(a)

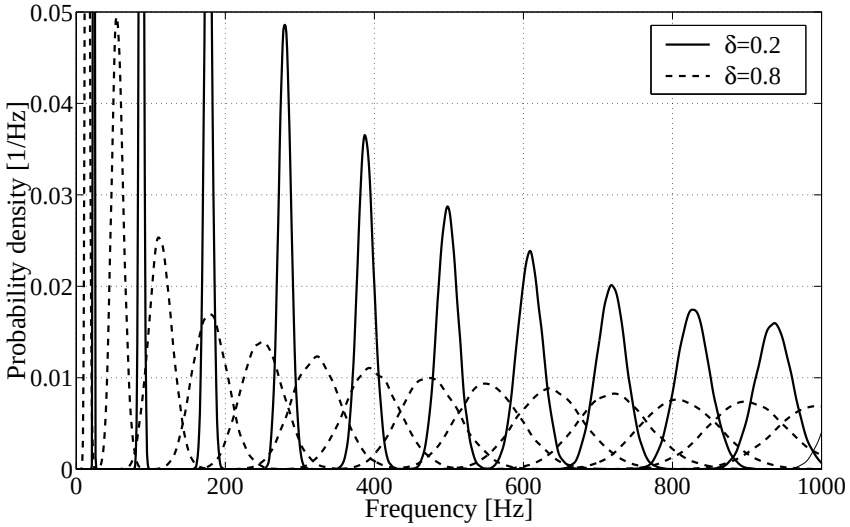

(b)

Fig. 2. Slender beam: (a) 50 lowest deterministic eigenfrequencies of the mean model, and mean of the random eigenfrequencies for δ=0.8 and $n_{\mathrm{T}} = 20$, $n_{\mathrm{T}} = 30$, $n_{\mathrm{T}} = 40$ and $n_{\mathrm{T}} = 50$, and (a) PDFs of the random eigenfrequencies between 0 and 1000 Hz for $\delta = 0.2$ and $\delta = 0.8$.

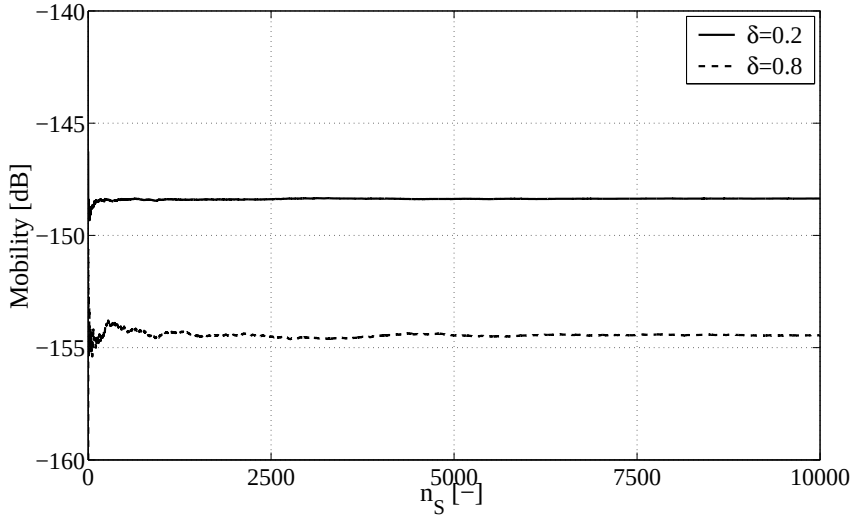

(a) 200 Hz.

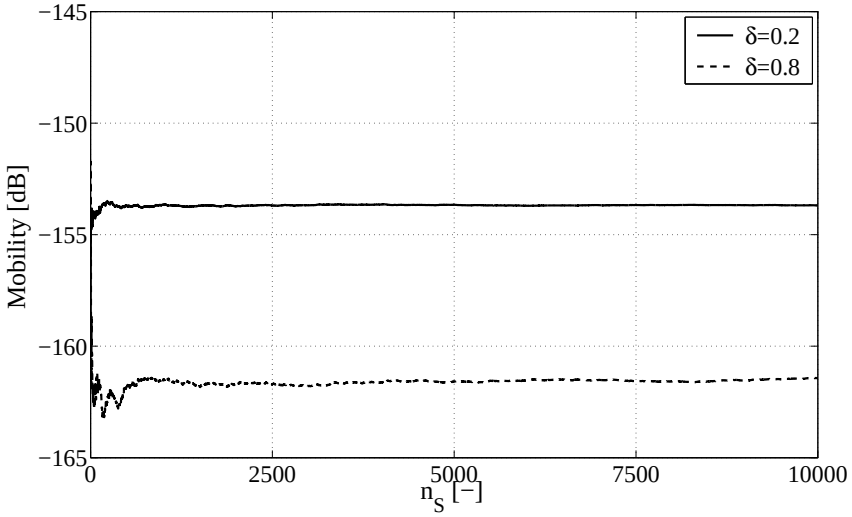

(b) 800 Hz.

Fig. 3. Slender beam: statistical mean of the realizations of the predicted random TF at $\boldsymbol{t}_2$ for $\delta = 0.2$ and $\delta = 0.8$ at frequencies (a) 200 Hz and (b) 800 Hz as a function of the number n_{S} of samples.

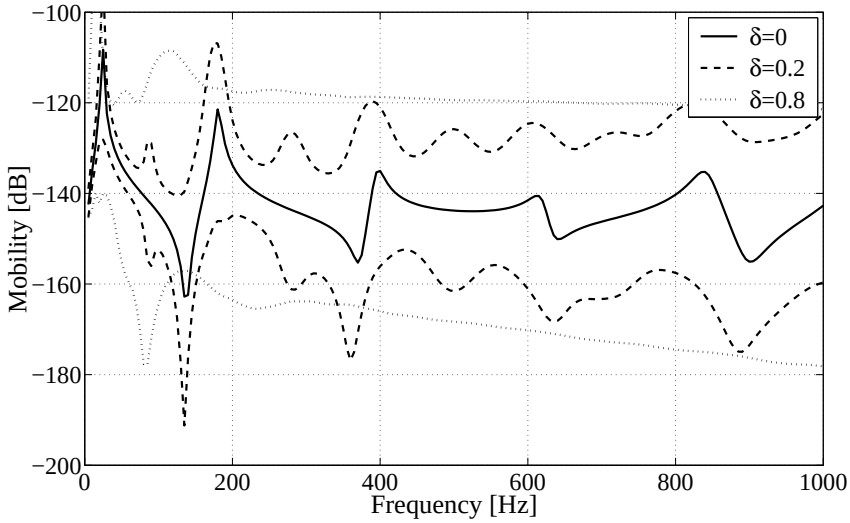

(a) TF at $\boldsymbol{t}_2$.

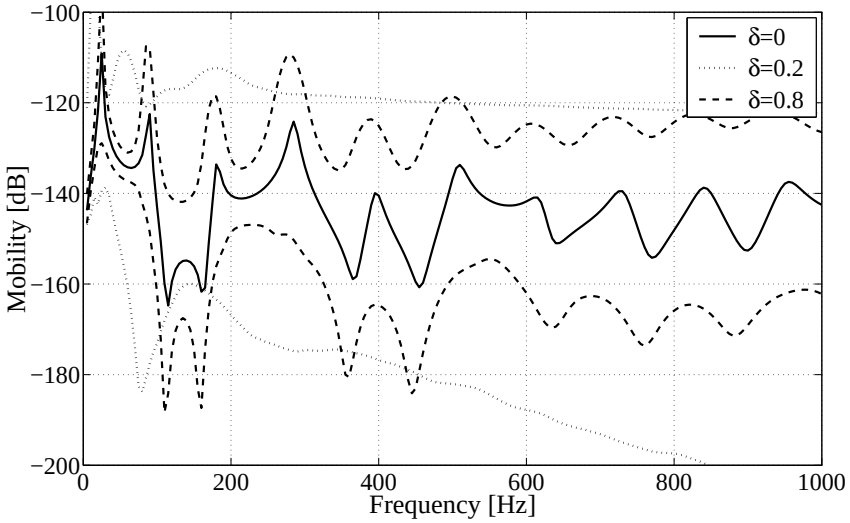

(b) TF at $\boldsymbol{t}_3$.

Fig. 4. Slender beam: amplitude of the TF predicted by the mean model, and 99%-confidence regions for the random TF for $\delta = 0.2$ and $\delta = 0.8$ at (a) $\boldsymbol{t}_2$ and (b) $\boldsymbol{t}_3$.

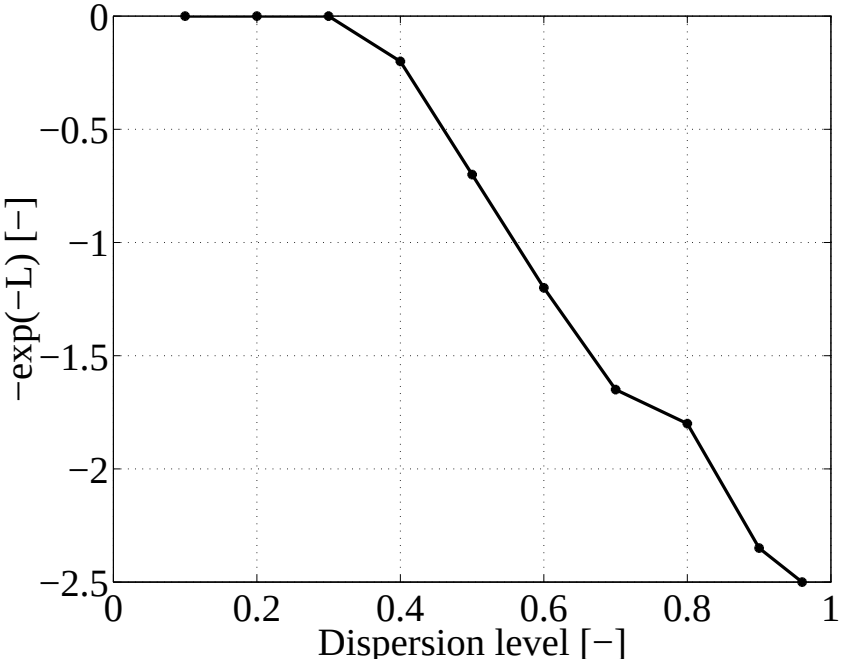

Fig. 5. Slender beam: distance $\mathcal{L}(\delta)$ as a function of δ.

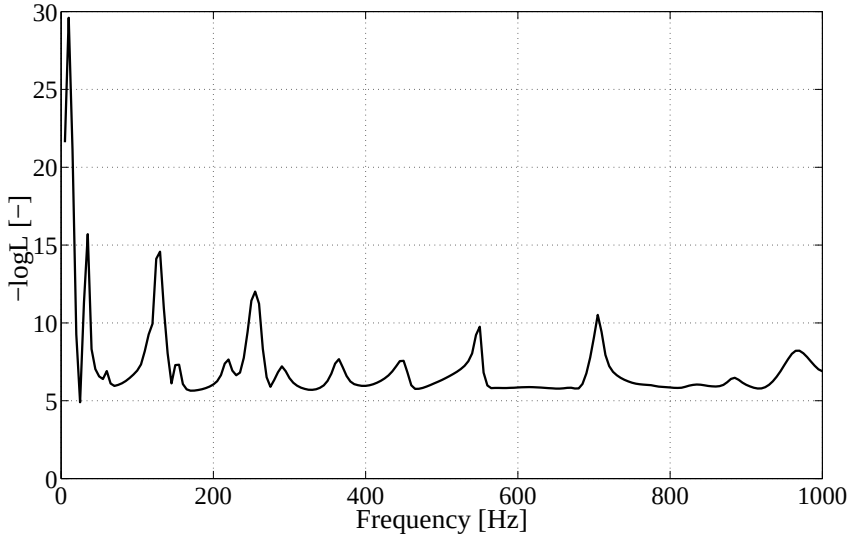

(a)

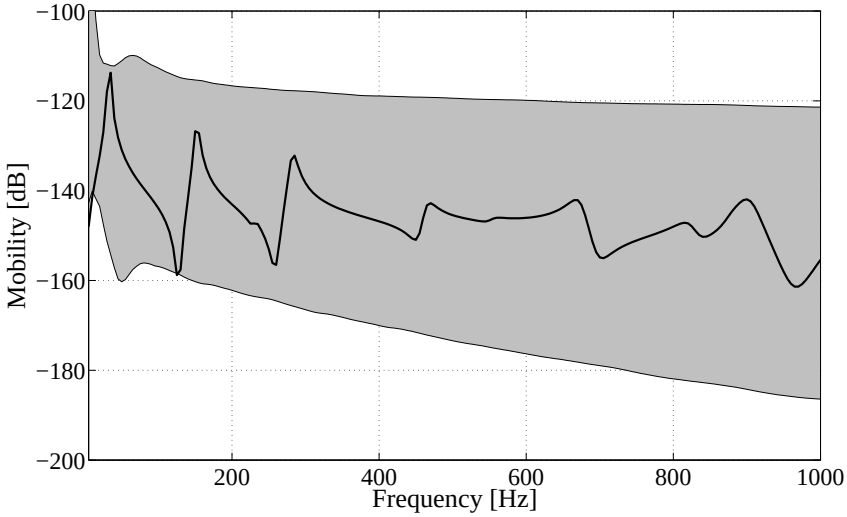

(b) TF at $\boldsymbol{t}_2$.

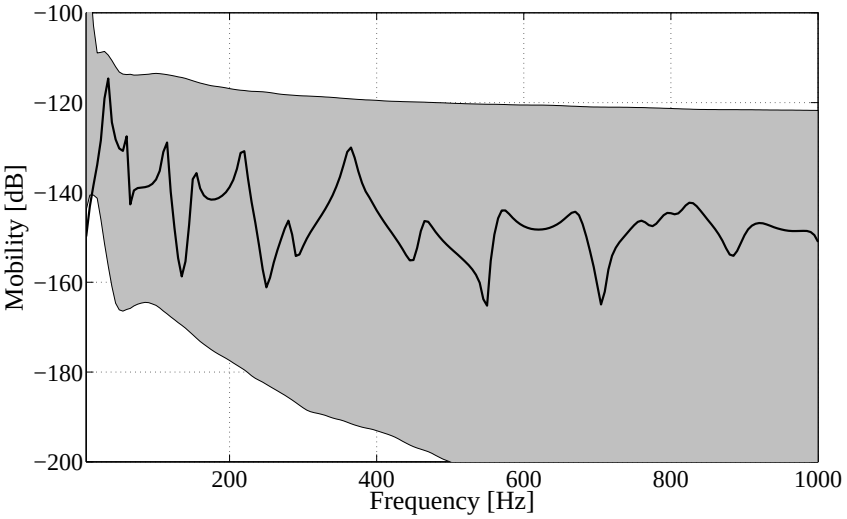

(c) TF at $\boldsymbol{t}_3$.

Fig. 6. Slender beam: (a) sign-reversed log-likelihood of $\hat{\delta} = 0.96$ as a function of the frequency and (b, c) amplitude of the observed TF (solid line) and 99%-confidence bounds for the identified random TF (grey patch) at $\boldsymbol{t}_2$ and $\boldsymbol{t}_3$.

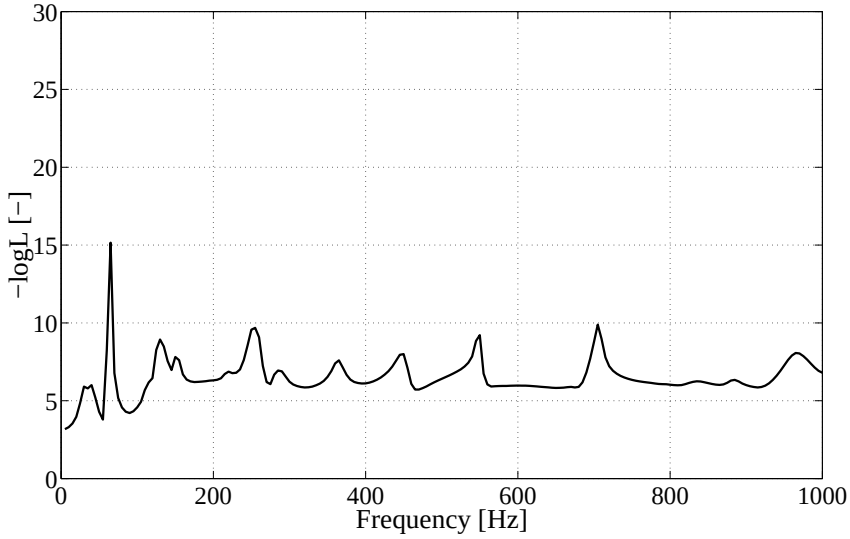

(a)

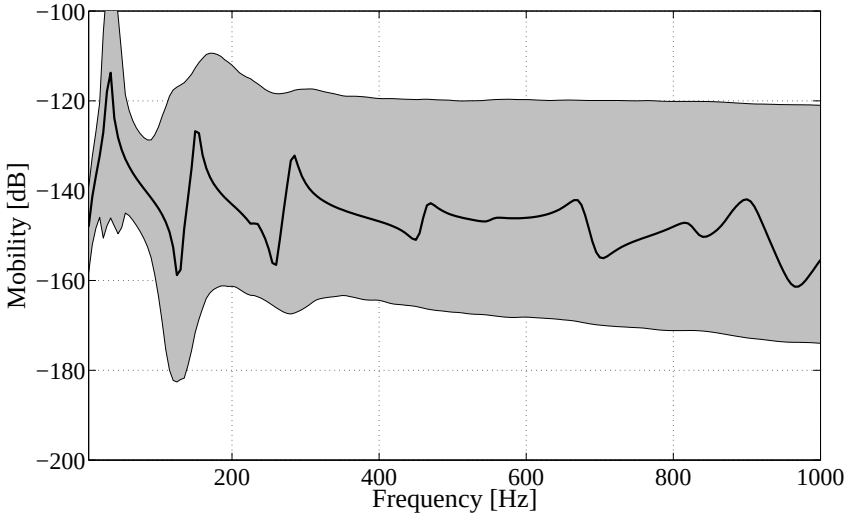

(b) TF at $\boldsymbol{t}_2$.

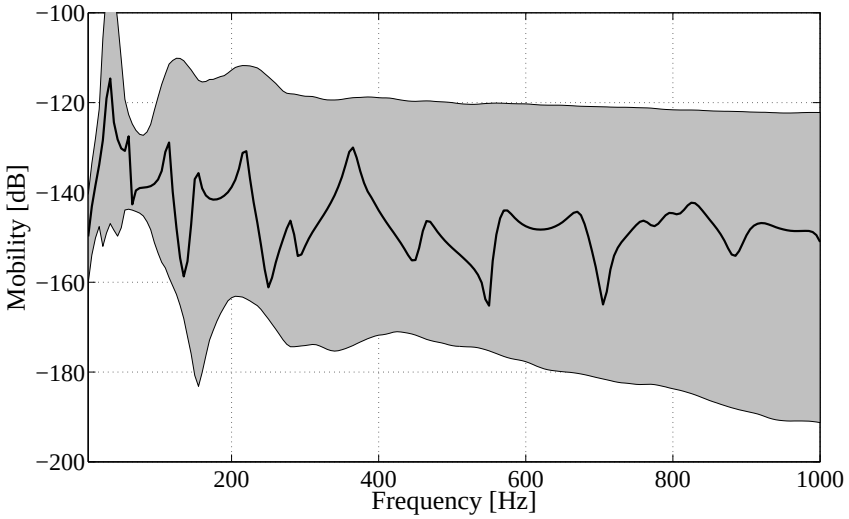

(c) TF at $\boldsymbol{t}_3$.

Fig. 7. Slender beam: (a) sign-reversed loglikelihood of $\hat{w}_1/2\pi = 46.67\,\text{Hz}$, $\hat{w}_2/2\pi = 172.63\,\text{Hz}$, $\hat{w}_3/2\pi = 230.00\,\text{Hz}$ and $\hat{\delta} = 0.67$ as a function of the frequency and (b, c) amplitude of the observed TF (solid line) and 99%-confidence bounds for the identified random TF (grey patch) at $\boldsymbol{t}_2$ and $\boldsymbol{t}_3$.

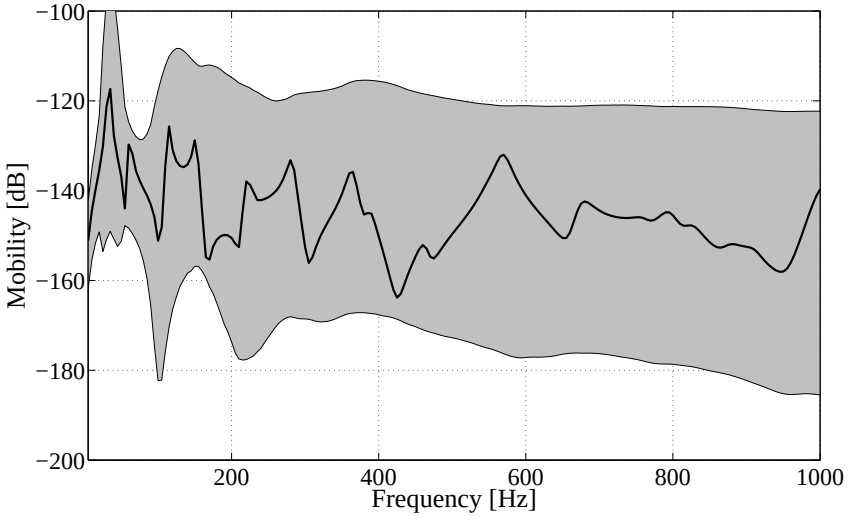

Fig. 8. Slender beam: amplitude of the TF predicted by the 3D FE model (solid line) and 99%-confidence bounds for the identified random TF (grey patch) at $\boldsymbol{t}_1$.

(a)

(b)

Fig. 9. Ground-borne vibrations in the Maison du Mexique: (a) tunnel at the station Gentilly and (b) side view of the Maison du Mexique.

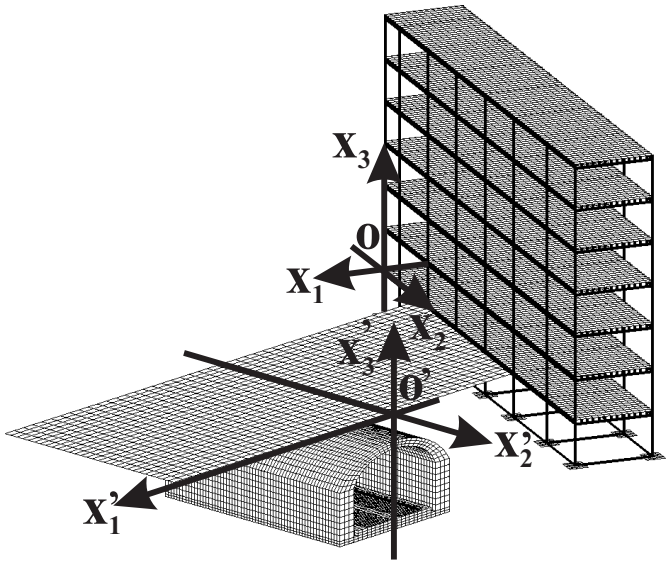

Fig. 10. Ground-borne vibrations in the Maison du Mexique: schematic overview of the site of Cité Universitaire.

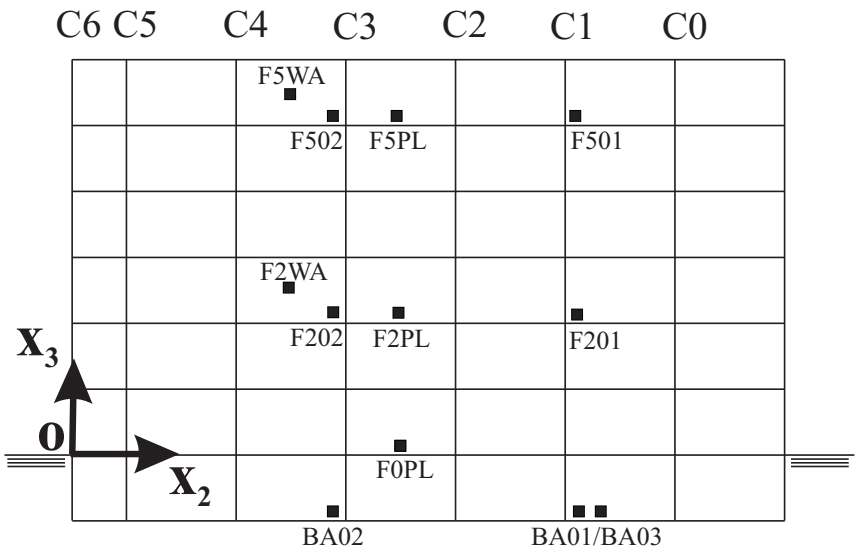

Fig. 11. Ground-borne vibrations in the Maison du Mexique: measurement locations.

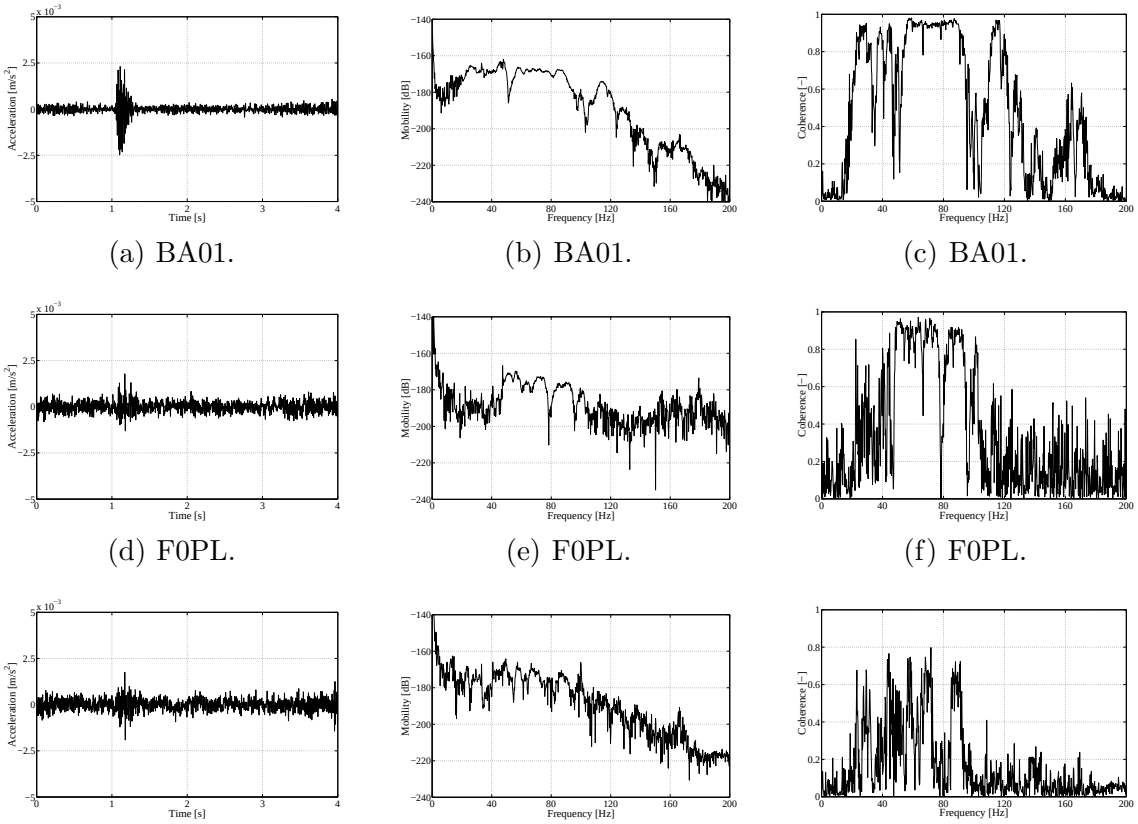

(a) BA01. (b) BA01. (c) BA01.

(d) F0PL. (e) F0PL. (f) F0PL.

(g) F201. (h) F201. (i) F201.

Fig. 12. Ground-borne vibrations in the Maison du Mexique: (a, d, g) time history of the measured acceleration during the sixth event, (b, e, h) amplitude of the estimated noise-free TF and (c, f, i) coherence function between the applied force and the measured response at BA01, F0PL and F201.

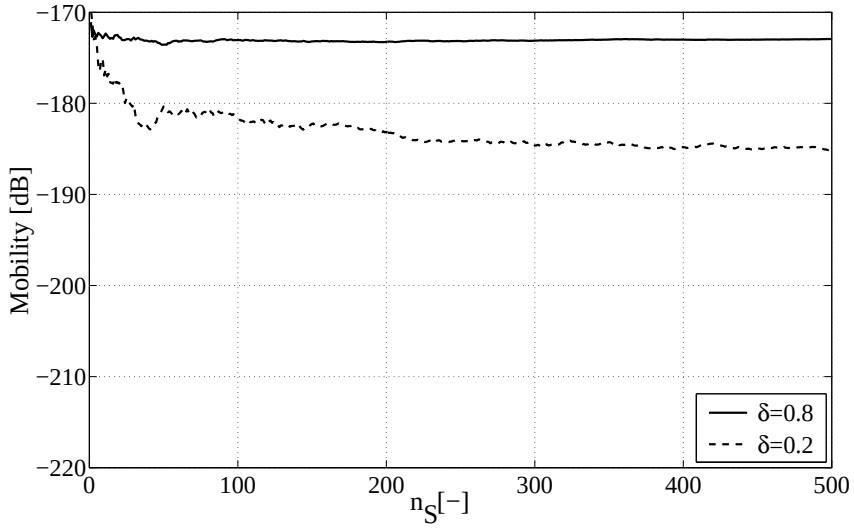

(a) 50 Hz.

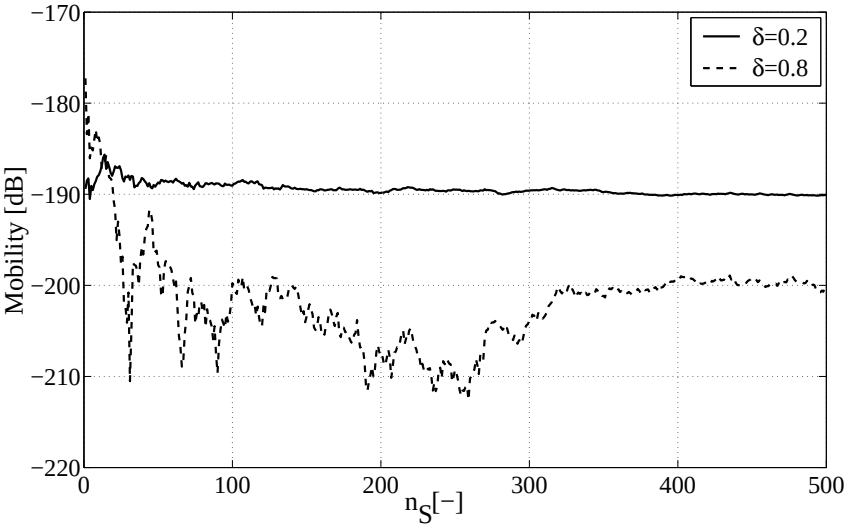

(b) 100 Hz.

Fig. 13. Ground-borne vibrations in the Maison du Mexique: statistical mean of the realizations of the predicted random TF at F0PL for $\delta = 0.2$ and $\delta = 0.8$ at frequencies (a) 50 Hz and (b) 100 Hz as a function of the number n_{S} of samples.

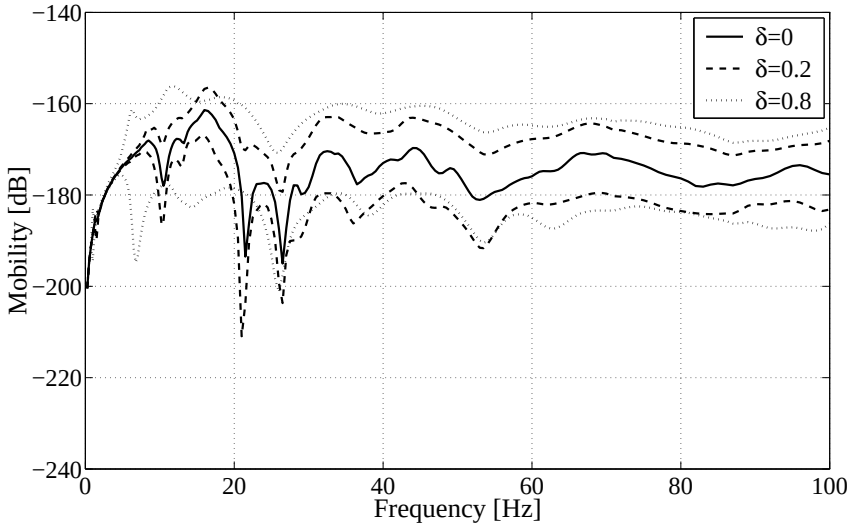

(a) TF at BA01.

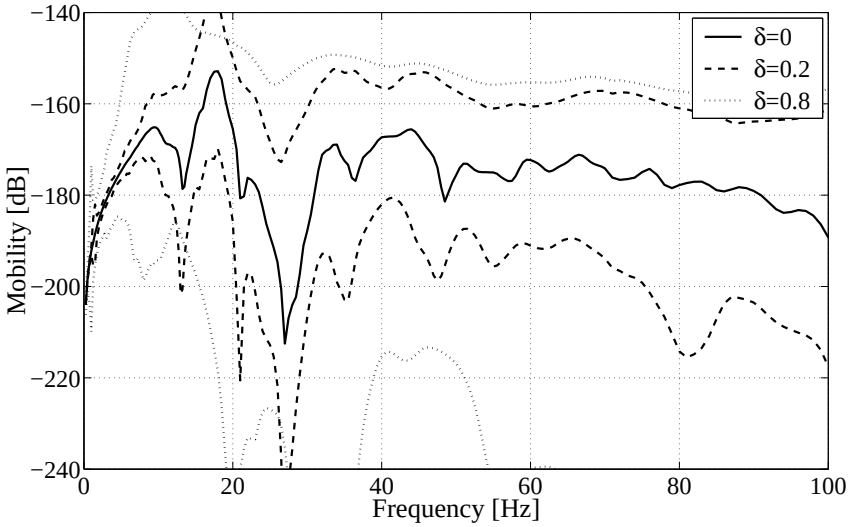

(b) TF at F0PL.

Fig. 14. Ground-borne vibrations in the Maison du Mexique: amplitude of the TF predicted by the mean model, and 99%-confidence regions for the random TF for $\delta = 0.2$ and $\delta = 0.8$ at (a) BA01 and (b) F0PL.

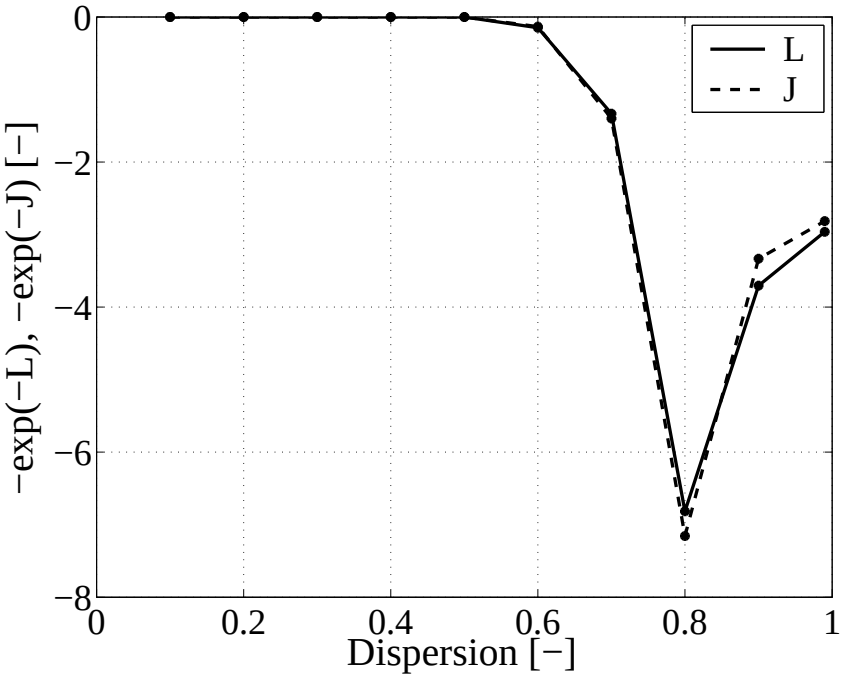

Fig. 15. Ground-borne vibrations in the Maison du Mexique: distances $\mathcal{L}(\delta)$ and $\mathcal{J}(\delta)$ as a function of δ.

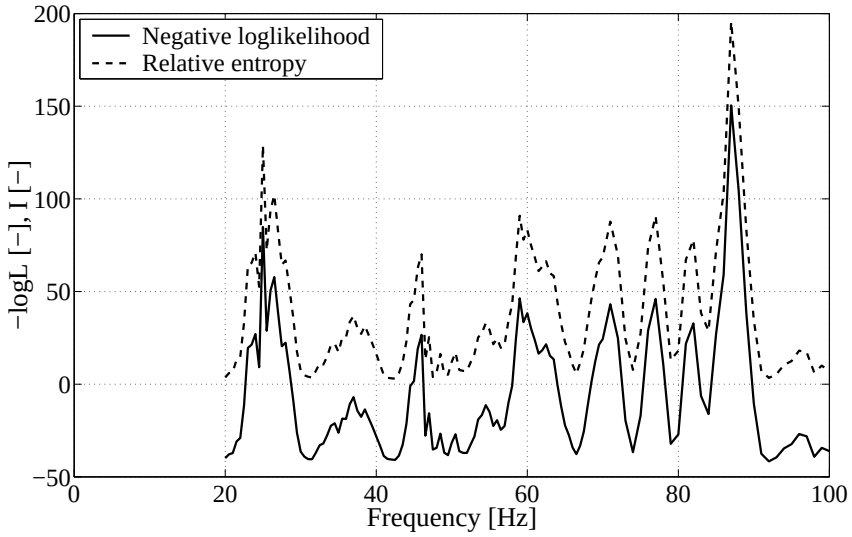

(a)

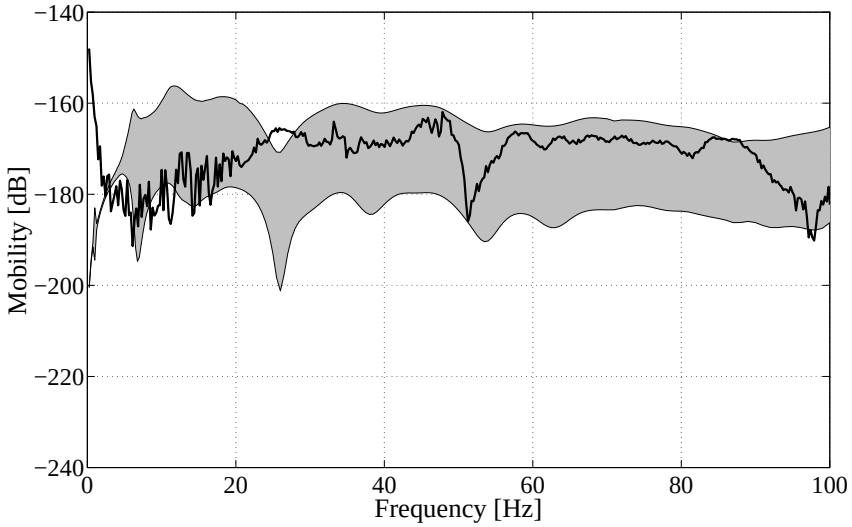

(b) TF at BA01.

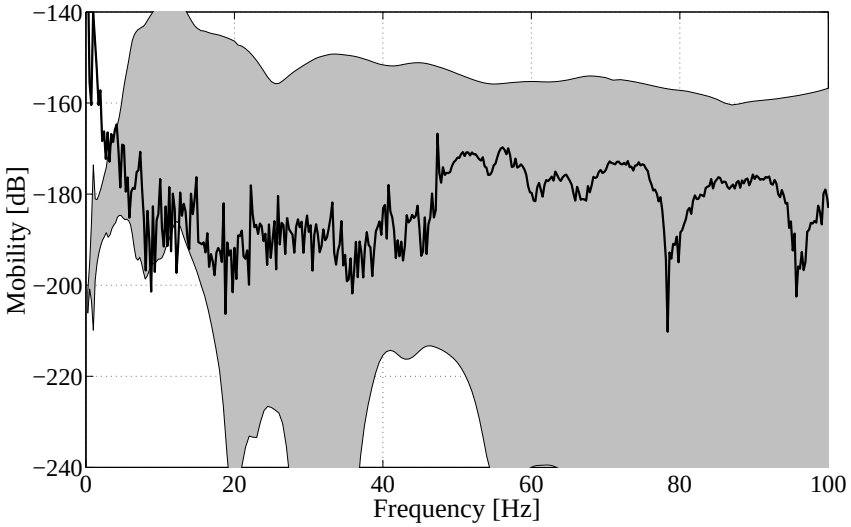

(c) TF at F0PL.

Fig. 16. Ground-borne vibrations in the Maison du Mexique: (a) sign-reversed loglikelihood (solid line) and relative entropy (dashed line) of $\hat{\delta} = 0.8$ as a function of the frequency and (b, c) amplitude of the estimated noise-free TF (solid line) and 99%-confidence bounds for the identified random TF (grey patch) at BA01 and F0PL.

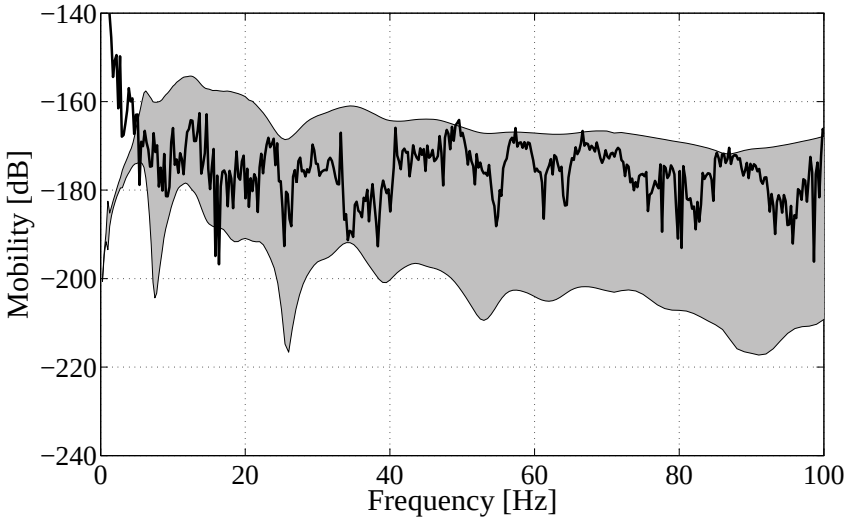

Fig. 17. Ground-borne vibrations in the Maison du Mexique: amplitude of the estimated noise-free TF (solid line) and 99%-confidence bounds for the identified random TF (grey patch) at F201.

List of Tables

Label	Location	Coordinates (x_1, x_2, x_3)
BA01	in the basement next to column C1	($-0.5\,\mathrm{m}$, $26.5\,\mathrm{m}$, $-3.6\,\mathrm{m}$)
F0PL	at the ground floor between columns C2 and C3	($-2.9\,\mathrm{m}$, $18.2\,\mathrm{m}$, 0)
F201	at the second floor right next to column C1	($-0.5\,\mathrm{m}$, $26.5\,\mathrm{m}$, $6.8\,\mathrm{m}$)

Table A.1
Ground-borne vibrations in the Maison du Mexique: measurement locations.